Order Number 1339068

Evaluation of correlated double sampling used with solid state imagers

Wang, Yi-Fu, M.S.

The University of Arizona, 1989

U·M·I
300 N. Zeeb Rd.
Ann Arbor, MI 48106

EVALUATION OF CORRELATED DOUBLE SAMPLING USED WITH SOLID STATE IMAGERS

by

Yi-Fu Wang

A Thesis Submitted to the Faculty of the

DEPARTMENT OF ELECTRICAL AND COMPUTER ENGINEERING

In Partial Fulfillment of the Requirements

For the Degree of

MASTER OF SCIENCE

WITH A MAJOR IN ELECTRICAL ENGINEERING

In the Graduate College

THE UNIVERSITY OF ARIZONA

1 9 8 9

STATEMENT BY AUTHOR

This thesis has been submitted in partial fulfillment of requirements for an advanced degree at The University of Arizona and is deposited in the University Library to be made available to borrowers under rules of the Library.

Brief quotations from this thesis are allowable without special permission, provided that accurate acknowledgement of source is made. Request for permission for extended quotation from or reproduction of this manuscript in whole or in part may be granted by the head of the major department or the Dean of the Graduate College when in his or her judgment the proposed use of the material is in the interests of scholarship. In all other instances, however, permission must be obtained from the author.

SIGNED: Yi-Fei Wang

APPROVAL BY THESIS DIRECTOR

This thesis has been approved on the date shown below:

Michael W. Marcellin
Assistant Professor of
Electrical and Computer Engineering

December 11, 1989
Date

ACKNOWLEDGMENTS

I would like to express my gratitude to Doctor Michael W. Marcellin for his guidance as my advisor for this work.

I am grateful to Doctor Eustace L. Dereniak for his encouragement, support, and providing the opportunity to work in his group four years ago. I am also grateful to Mr. Dave Perry at Optical Detection Lab for his valuable assistance and technical discussions.

Many thanks to Miss Yee-Hwa Jessica Rao for her support and skillful typing of the manuscript.

Finally, I wish to dedicate my work to my parents, without their support, understanding, and love I would never have accomplished my research.

TABLE OF CONTENTS

LIST OF FIGURES

ABSTRACT

Correlated double sampling (CDS) is a widely used signal processing technique for removal of the Nyquist (reset) noise which is associated with charge sensing circuits employed in a solid state imager. In this thesis work, the power spectral density at the output of a correlated double sampling circuit with first-order low-pass filtered white noise at the input is calculated. A circuit constructed with discrete elements is made to simulate the output stage of a charge-coupled device (CCD). A low-pass filtered wide-band noise from a noise generator is added to the reset reference level when the output signal from this simulator is sampled by the correlated double sampling technique. The experiment measurements show that only about 10% of the noise power measured by simple sampling is obtained when CDS is employed. An autoregressive (AR) model is assumed to fit the sampled data and a recursive algorithm, based on least-squares solutions for the AR parameters using forward and backward linear prediction, is adopted for spectrum estimation. Some conclusions on choosing the bandwidth of the low pass filter for optimum operation is also included.

CHAPTER I INTRODUCTION

1-1 INTRODUCTION

Solid state imaging systems using charge-coupled devices (CCD's) are commonly used in fields such as astronomy, where low light levels are encountered. In these applications the CCD is normally cooled to less than 200 ^{o}K so that its dark current is negligible and the main noise sources are associated with the readout circuitry. A technique, known as correlated double sampling (CDS), can be used to remove the reset noise and suppress the low-frequency noise to provide low-noise signal processing of the video signal. In this work, a simulative readout circuit is used to evidence the removal of reset noise, and the suppression of low frequency noise is proven mathematically.

1-2 BACKGROUND

CCD imagers are arrays of MOS (Metal Oxide Silicon) capacitors fabricated in a single crystal of silicon. Charge generated by photons absorbed in the silicon substrate is collected in potential wells formed under each capacitor electrode when a voltage is applied. By manipulation of the electrode voltages, the stored charge can be

shifted sequentially from one capacitor to the next. It can be arranged that the serial train of charge packets (one packet from each pixel) is presented to a single charge sensing circuit which generates the output waveform.

Floating diffusion is the most commonly used technique for constructing an output circuit. This technique is used in presently available solid state imagers. In the floating diffusion technique, a charge packet is dumped onto the capacitance (C_{FD}) of a reverse biased diode and the resultant change in voltage is sensed by an on-chip MOS source follower amplifier. Before each pixel is read, the capacitor must be reset to a reference voltage. The noise introduced by this resetting will have a r.m.s. voltage value of[1] $(kT/C_{FD})^{1/2}$, where k is Boltzmann's constant and T is the temperature. For T = 77 ^{o}K and C_{FD} = 0.1 pF (a typical value) this noise amounts to the r.m.s. noise voltage of ~0.1 mV. This reset noise is usually removed by taking the difference between samples of the CCD output voltage before and after the signal charge is sensed; this technique is known as correlated double sampling.

In modern CCD's, the signal charge is stored in a buried channel remote from trapping centers in the surface oxide layer and the noise associated with charge transfer is negligible. If care is taken with the layout of external circuitry and low noise off-chip amplifiers are

used, then the major noise source (assuming the CCD is cooled) is the on-chip MOS amplifier.

There are two noise sources in a MOS field-effect transistor (FET) amplifier, namely thermal channel noise and $1/f$ flicker noise[1]. Since $1/f$ noise in MOSFETs is believed to be due to trapping in surface states, substantial reduction in $1/f$ noise can be obtained if these transistors are operated in a buried channel mode (i.e., the signal is away from the Si-SiO2 interface). The r.m.s. value of the thermal noise voltage of the channel of a MOSFET is given by[2] $(4kT\Delta BR)^{1/2}$, where k is the Boltzmann's constant, T is the temperature, ΔB is the bandwidth and R is the channel resistance. For T = 77 ^{o}K, ΔB = 5 MHz and R = 10^4 Ω, this thermal channel noise has a r.m.s. noise voltage of ~15 μV. Therefore, this thermal noise is considered to be negligible compared with the reset noise. Thus, this work will concentrate primarily on techniques that reduce the reset noise.

CHAPTER II THEORY

2-1 NOISE

It is usually found that noise is composed of randomly occurring voltages which are unrelated in phase or frequency. On close examination, noise voltages show pulse-like waveforms, some with large peaks, which occur quite randomly and continuously.

Mathematical concepts used in the evaluation of noise relate either to noise voltages or to noise power spectral density. Since noise fluctuations are both positive and negative, the mean-square noise voltage is first determined, which then leads to the expression of a.c. noise power $P_n = \overline{V_n^2}/R$ where $(\overline{V_n^2})^{1/2}$ is the r.m.s. noise voltage and R is the circuit resistance involved. Alternatively, it is sometimes more convenient to consider the spectral distribution of the noise present, and to evaluate its spectral density $S(f)$ in a given bandwidth df.

Since the noise power delivered to a load depends on the load resistance, it is necessary to define the exact nature of the noise power calculated. In practice, it is most usual to define the noise as the available noise power, i.e. the maximum noise power available in the load under matched conditions.

The average noise power or the mean-square noise voltage can be evaluated for a load resistance of 1 Ω by the use of integration. The power spectral density function $S(f)$ is defined as the average power at frequency f in a 1 Ω load resistor. Hence, $S(f)df$ gives the average power in the infinitesimal frequency range df and so the average power P_{av} in the random noise signal is given by

$$P_{av} = \int_{-\infty}^{\infty} S(f)df. \qquad (2\text{-}1)$$

Many random noise signals generated by various sources are known to have a uniform power distribution over a very wide range of frequencies up to about 10^{13} Hz, which is in the ultra-violet range, after which it falls off as predicted by quantum theory. Such noise is defined as white noise by analogy with white light, which covers a broad band of frequencies. The nearest examples are thermal noise in a resistor and shot noise in transistors.

2-2 Autocorrelation Function

In the study of many random processes such as noise, it is of interest to know whether there is any statistical regularity or correlation in the random process. Also, random functions do not lend themselves to Fourier methods for analysis, so the autocorrelation function for handling these functions is necessary to characterize these noise process.

An autocorrelation function, which is a measure of the regularity of the specified function, is analytic, and its Fourier transform has an important physical interpretation. The possibility of correlation between two random variables leads to the notion of the autocorrelation function which endeavors to correlate a random signal $x(t)$ with itself but delayed by a time interval τ, i.e. $x(t-\tau)$. The autocorrelation function $R_{xx}(\tau)$ is defined as

$$R_{xx}(\tau) = \lim_{T\to\infty} \frac{1}{T} \int_{-T/2}^{T/2} x(t)x(t-\tau)dt \qquad (2\text{-}2)$$

where the definition applies to all forms of signals either random or periodic (deterministic).

The process of finding $R_{xx}(\tau)$ implies the multiplication of $x(t)$ with the delayed signal $x(t-\tau)$ and averaging the result over the time interval T. Since τ is variable, it leads to different values of $R_{xx}(\tau)$. Of particular interest is the value $R_{xx}(0)$ when $\tau=0$. For example, if $x(t)$ is used to represent the voltage value of a random noise signal, then

$$R_{xx}(0) = \lim_{T\to\infty} \frac{1}{T} \int_{-T/2}^{T/2} x(t)x(t)dt$$

or

$$R_{xx}(0) = \lim_{T\to\infty} \frac{1}{T} \int_{-T/2}^{T/2} x^2(t)dt \qquad (2\text{-}3)$$

is the mean square voltage of the random noise signal or the average noise power delivered to a 1 Ω load resistor.

2-3 Power Spectral Density

To obtain the average power P_{av} associated with a periodic or random signal $x(t)$ which extends over an indefinite period of time t, it is assumed that the average power must be finite. The evaluation is based on the power spectral density function $S(f)$ which is defined as the average power density at frequency f in a 1 Ω load resistor. Hence, $S(f)df$ gives the average power in the infinitesimal frequency range df and so the average power P_{av} in the periodic or random signal $x(t)$ is given by eq. (2-1)

$$P_{av} = \int_{-\infty}^{\infty} S(f)df = \frac{1}{2\pi}\int_{-\infty}^{\infty} S(\omega)d\omega.$$

An important relationship between the autocorrelation function $R_{xx}(\tau)$ and the spectral density function $S(f)$ is given by the Wiener-Khintchine theorem[3] which states that $R_{xx}(\tau)$ and $S(f)$ form a set of Fourier transform pairs given by

$$S(f) = \int_{-\infty}^{\infty} R_{xx}(\tau)e^{-j2\pi f\tau}d\tau \qquad (2\text{-}4)$$

$$R_{xx}(\tau) = \int_{-\infty}^{\infty} S(f)e^{j2\pi f\tau}df. \qquad (2\text{-}5)$$

2-4 Noise Transfer Characteristics of a Correlated Double Sampling Circuit

The correlated double sampling operation is performed in two phases: 1) clamp, e.g., sampling of a reference value and noise at T_1 and 2) sampling of the disturbed signal with the clamped value subtracted at T_2. If the noise at the clamp and sampling times is correlated, this signal-processing scheme can result in an effective noise reduction.

For analytical purposes, the implementation of the correlated double sampling (CDS) circuit and delay-subtractor model shown in Fig. 2-1 will be considered. The delay block represents an ideal analog delay line having a delay of $\Delta\tau$ seconds. The delayed signal is subtracted from the direct signal, and the net difference is sampled to yield the output.

If the input to the RC lowpass filter as shown in Fig. 2-2 is white noise with a power spectral density of S_w (V^2/Hz), then the input to the CDS circuit will be a first-order lowpass filtered noise with a power spectral density $S_{1p}(f)$ (V^2/Hz).

If $H(f)$ is the network transfer function of the RC lowpass filter, we have

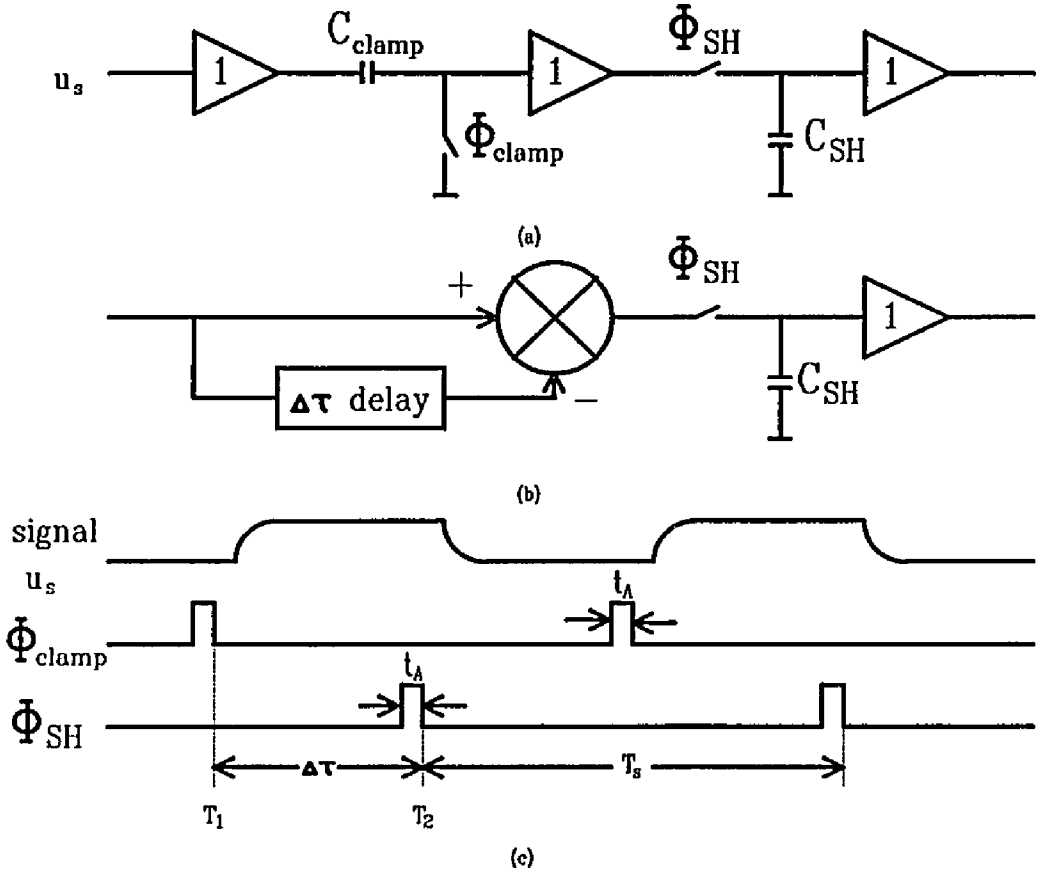

Fig. 2-1 Correlated double sampling.

(a) Practical realization, (b) Delay-subtractor model, (c) Timing

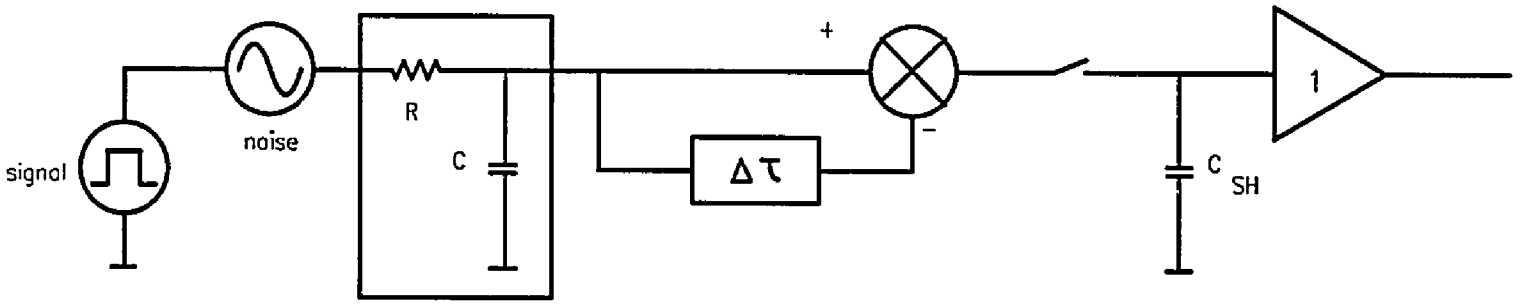

Fig. 2–2 Circuit with first–order noise source and CDS.

$$H(f) = \frac{1}{1+j(f/f_o)} \tag{2-6}$$

or

$$|H(f)|^2 = \frac{1}{1+(f/f_o)^2} \tag{2-7}$$

where $f_o = 1/(2\pi RC) = 1/(2\pi\tau_o)$ is the cutoff frequency and $\tau_o = RC$ is the time constant of the lowpass filter.

If S_w and $S_{ip}(f)$ are the input and output power spectral densities of the lowpass filter, respectively, then

$$\frac{S_{out}(f)}{S_{in}(f)} = \frac{S_{ip}(f)}{S_w} = |H(f)|^2 = \frac{1}{1+(f/f_o)^2}$$

or

$$S_{ip}(f) = \frac{S_w}{1+(f/f_o)^2} \tag{2-8}$$

and the average noise power, $\overline{V_{ip}^2}$, at the output of the RC lowpass filter is given by

$$\begin{aligned}\overline{V_{ip}^2} &= \int_{-\infty}^{\infty} S_{ip}(f)df \\ &= S_w \cdot \int_{-\infty}^{\infty} \frac{df}{1+(f/f_o)^2} \\ &= \pi \cdot S_w \cdot f_o\end{aligned}$$

or

$$\overline{V_{ip}^2} = \frac{S_w}{2RC} = 2S_wB \tag{2-9}$$

where B is the noise bandwidth of the single pole RC filter, B = 1/4RC.

The autocorrelation function, $R_{Ip}(\tau)$, of the band-limited noise can be found by taking the inverse Fourier transformation of the power spectrum $S_{Ip}(f)$,

$$R_{Ip}(\tau) = \int_{-\infty}^{\infty} S_{Ip}(f)e^{j2\pi f\tau}df = S_{w\pi fo}\cdot\exp(-|\tau|/\tau_o) \qquad (2\text{-}10)$$

or

$$R_{Ip}(\tau) = R_{Ipo}\cdot\exp(-|\tau|/\tau_o) \qquad (2\text{-}11)$$

where $R_{Ipo} = R_{Ip}(0) = S_{w\pi fo} = \overline{V_{Ip}^2}$ is the average noise power at the output of the RC low-pass filter.

The r.m.s. output voltage at the delay-subtractor output, V_{ds}, is the difference in the input voltage level, $V_{Ip}(t)$, at two points in time separated by a time interval $\Delta\tau$, which is given by (see Appendix A)

$$\overline{V_{ds}^2} = \lim_{T\to\infty}\frac{2}{T}\int_{-T/2}^{T/2}\left[V_{Ip}(t)\right]^2 dt - \lim_{T\to\infty}\frac{2}{T}\int_{-T/2}^{T/2} V_{Ip}(t)\cdot V_{Ip}(t-\Delta\tau)dt \qquad (2\text{-}12)$$

where it has been assumed that $V_{Ip}(t)$ is stationary. Using the definition of an autocorrelation function

$$R_{Ip}(\tau) = \lim_{T\to\infty}\frac{1}{T}\int_{-T/2}^{T/2} V_{Ip}(t)V_{Ip}(t-\tau)dt,$$

$\overline{V_{ds}^2}$ can be rewritten as

$$\overline{V_{ds}^2} = 2[R_{Ip}(0)-R_{Ip}(\Delta\tau)]. \qquad (2\text{-}13)$$

Substituting eq.(2-11) into eq.(2-13) the following result is obtained:

$$\begin{aligned}\overline{V_{ds}^2} &= 2[R_{lpo}-R_{lpo}\cdot\exp(-\Delta\tau/\tau_o)] \\ &= 2R_{lpo}[1-\exp(-\Delta\tau/\tau_o)] \\ &= 2\overline{V_{lp}^2}[1-\exp(-\Delta\tau/\tau_o)] \qquad (2\text{-}14) \\ &= \text{the average noise power at the output} \\ &\quad \text{of the delay-subtractor.}\end{aligned}$$

If $H_{ds}(f)$ is the transfer function of the delay-subtractor modeling the clamp operation, the noise power spectrum $S_{ds}(f)$ can be written as

$$S_{ds}(f) = S_{lp}(f)|H_{ds}(f)|^2 \qquad (2\text{-}15)$$

with $|H_{ds}(f)|^2 = 2(1-\cos 2\pi f\Delta\tau)$, (see Appendix B).

Substituting eq. (2-8) into eq. (2-15) we have

$$\begin{aligned}S_{ds}(f) &= \frac{S_w}{1+(f/f_o)^2}[2(1-\cos 2\pi f\Delta\tau)] \\ &= \frac{2S_w(1-\cos 2\pi f\Delta\tau)}{1+(f/f_o)^2}\,. \qquad (2\text{-}16)\end{aligned}$$

The autocorrelation function of the noise at the delay-subtractor output is (see Appendix C)

$$R_{ds}(\tau) = 2R_{lp}(\tau)-R_{lp}(\tau+\Delta\tau)-R_{lp}(\tau-\Delta\tau). \qquad (2\text{-}17)$$

By using eq. (2-11), $R_{ds}(\tau)$ can be rewritten as

$$R_{ds}(\tau) = R_{lpo}[2\exp(-|\tau|/\tau_o)-\exp(-|\tau+\Delta\tau|/\tau_o)-\exp(-|\tau-\Delta\tau|/\tau_o)]. \qquad (2\text{-}18)$$

Assuming an ideal (Dirac) sampler with zero hold time is used for the sample and hold operation at the output of the CDS circuit, the voltage at the output of the CDS circuit, V_{icds}, can be represented by the multiplication of V_{ds} with a Dirac comb δ_T:

$$V_{icds}(t) = V_{ds}(t) \sum_{n=-\infty}^{\infty} \delta(t-nT_s) = V_{ds}(t)\delta_{Ts} \qquad (2\text{-}19)$$

where T_s is the sampling period. Since V_{ds} and $\delta_{Ts}(t)$ are independent, the autocorrelation function of the sampled noise voltage, $V_{icds}(t)$, is given by[4]

$$R_{icds}(\tau) = R_{Ts}(\tau)R_{ds}(\tau)$$

$$= \frac{1}{T_s}\delta_{Ts}(\tau)R_{ds}(\tau) \qquad (2\text{-}20)$$

where $R_{Ts}(\tau)$ and $R_{ds}(\tau)$ are the autocorrelation functions of $\delta_{Ts}(t)$ and $V_{ds}(t)$, respectively. Furthermore, the power spectral density S_{icds}, after ideal sampling, is the Fourier transformation of eq. (2-20):

$$S_{icds}(f) = \frac{1}{T_s} \int_{-\infty}^{\infty} \delta_{Ts}(\tau)R_{ds}(\tau)\exp(-j2\pi f\tau)d\tau$$

$$= \frac{1}{T_s} \sum_{n=-\infty}^{\infty} R_{ds}(nT_s)\exp(-j2\pi fnT_s) \qquad (2\text{-}21)$$

which after some calculations and hyperbolic transformations (see Appendix D), leads to the solution

$$S_{icds}(f) = \frac{2R_{ipo}}{T_s}\left[\frac{\sinh(\beta)\cdot[\cosh(\beta\gamma)-1]}{\cos(2\pi fT_s)-\cosh(\beta)} + \sinh(\beta\gamma)\right] \qquad (2\text{-}22)$$

or

$$S_{icds}(f) = \frac{S_w}{\tau_o T_s}\left[\frac{\sinh(\beta)\cdot[\cosh(\beta\gamma)-1]}{\cos(2\pi fT_s)-\cosh(\beta)} + \sinh(\beta\gamma)\right] \qquad (2\text{-}23)$$

where τ_o = RC = time constant of the low-pass filter

f_s = sampling frequency

T_s = $1/f_s$ = sampling period

$\Delta\tau$ = time interval delayed by the delay-subtractor

β = T_s/τ_o

= ratio of sampling period to low pass filter time constant

γ = $\Delta\tau/T_s$

= ratio of delayed time to one sampling period.

Moreover, in practical cases a signal is sampled and held with a hold time t_A. Thus the expression of the output spectral density S_{icds} will be damped by a $[\sin(\pi x)/(\pi x)]^2$ function[4]:

$$S_{cds}(f) = S_{icds} \cdot t_A^2 \cdot \mathrm{sinc}^2(f t_A)$$

$$= S_w \alpha^2 \beta \cdot \left[\frac{\sinh(\beta)\cdot[\cosh(\beta\gamma)-1]}{\cos(2\pi f T_s)-\cosh(\beta)} + \sinh(\beta\gamma) \right] \cdot \mathrm{sinc}^2(\alpha f/f_s) \qquad (2\text{-}24)$$

where t_A = hold time of sampler

α = t_A/T_s = duty cycle

$\mathrm{sinc}(x)$ = $\sin(\pi x)/(\pi x)$.

In summary, if a single-pole lowpass filtered white noise with power spectral density S_w is presented at the input of the CDS circuit, then the output power spectral density can be expressed as

$$S_{cds}(f) = S_w \alpha^2 \beta \cdot \left[\frac{\sinh(\beta)\cdot[\cosh(\beta\gamma)-1]}{\cos(2\pi f T_s)-\cosh(\beta)} + \sinh(\beta\gamma) \right] \cdot \mathrm{sinc}^2(\alpha f/f_s).$$

Fig. 2-3 shows computer generated plots of the spectral density S_{cds} normalized with respect to the $sinc^2$ function as a function of frequency f/f_s for different ratios of sampling time to filter time constant $\beta = T_s/\tau_o$ as parameter, where

$$S_n(f) = S_{cds}(f)/[S_w \cdot \alpha^2 \cdot sinc^2(\alpha f/f_s)]$$

$$= \beta \cdot \left[\frac{\sinh(\beta) \cdot [\cosh(\beta\gamma)-1]}{\cos(2\pi f T_s)-\cosh(\beta)} + \sinh(\beta\gamma) \right] \qquad (2\text{-}25)$$

is the normalized power spectrum.

In Fig. 2-3, the output-noise spectrum $S_n(f)$ of the CDS circuit has a "whitened" shape (for large β) due to aliasing of the band-limited input noise. The normalized output-noise spectrum remains relatively flat even at $\beta \ll 2$ for $\gamma = 0.5$. It is also interesting to note that for $\beta < 2$, the power spectral density of the noise is attenuated at low frequencies. According to the transfer function of CDS $|H_{ds}(f)|^2 = 2(1-\cos 2\pi f \Delta\tau)$, which is derived in Appendix B, noise at frequencies that are much less than $1/\Delta\tau$ can be substantially suppressed. This characteristic of CDS is especially effective in suppressing the $1/f$ noise contributed by the on-chip MOS source follower amplifier as long as the $1/f$ corner frequency of this MOS amplifier is sufficiently low.

For $\gamma \leq 0.5$, the normalized CDS output-noise spectrum at one-half the sampling frequency (i.e., $S_n(0.5f_s)$) is plotted in Fig. 2-4 for a

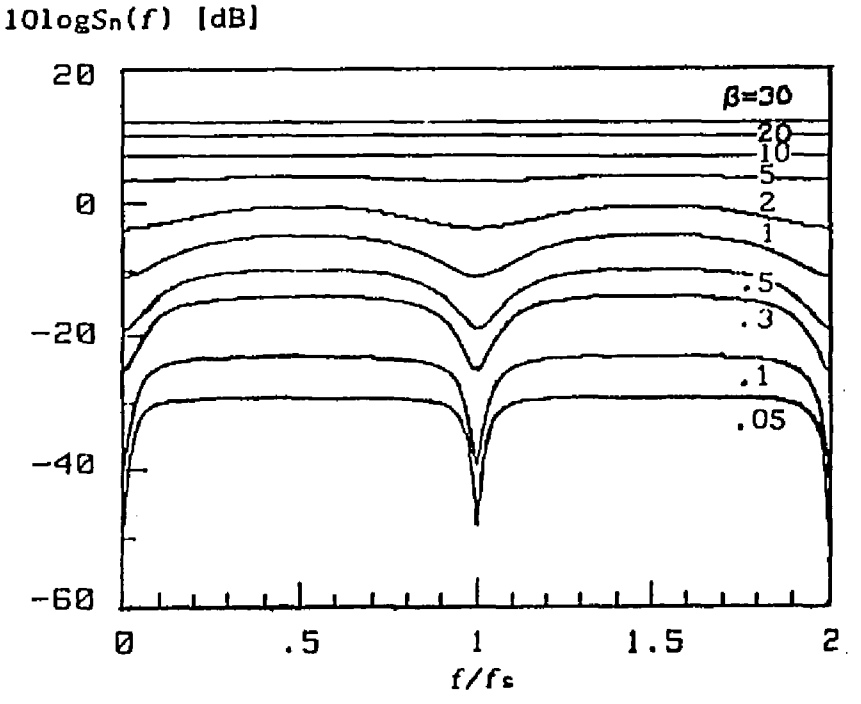

Fig. 2-3 Normalized Output-Noise Power Spectral Density (Eq. 2-25) as a Function of f/f_s, Parameters $\alpha=0.05$, $\beta=T_s/\tau_o$, $\gamma=0.5$.

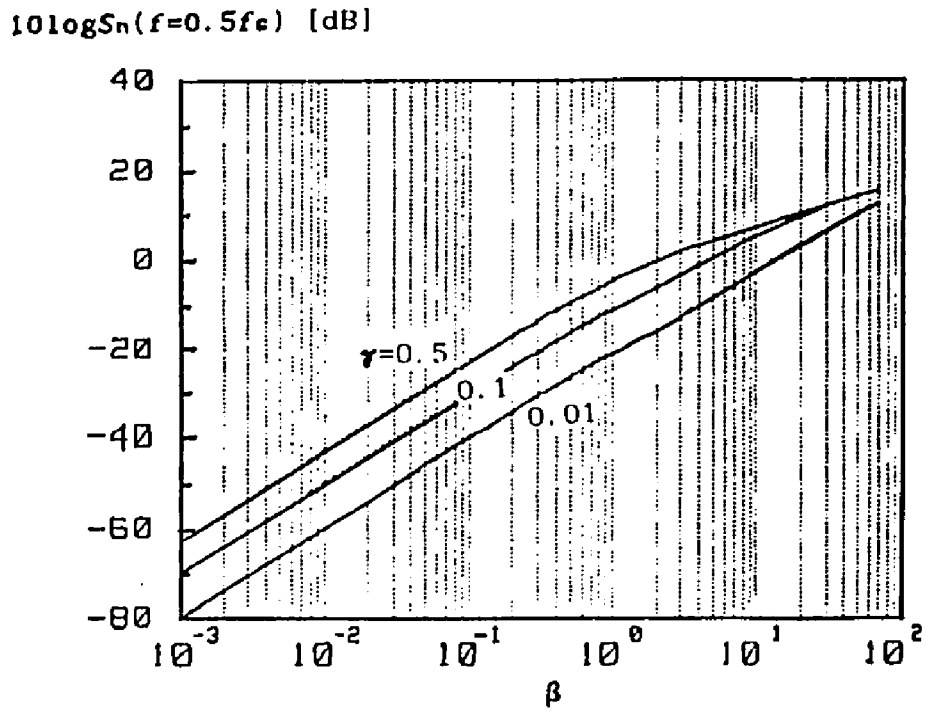

Fig. 2-4 Normalized Output-Noise Power Spectral Density as a Function of T_s/τ_o, Parameters α=0.05, $\beta=T_s/\tau_o$, $\gamma=\Delta\tau/T_s$.

fixed sampling rate f_S. The power spectral density of the noise increases proportionally to the bandwidth $B = 1/4\tau_0$ of the input noise for undersampling ($\beta > 2$), while it demonstrates clearly the good noise reduction properties of the circuit for oversampling ($\beta < 2$).

CHAPTER III APPROACH

3-1 Operation of a Charge Coupled Device

As mentioned in Chapter 1, a charge coupled device (CCD) is a metal-oxide-semiconductor (MOS) structure, as shown in Fig. 3-1, which can collect and store minority-carrier charge packets in localized potential wells at the Si-SiO2 interface. The CCD can transfer charge packets in discrete-time increments via the controlled movement of potential wells. The charge packets can then be detected at the output via capacitive coupling. A charge coupled device acts as an analog shift register composed of three sections.

(1) The input section which contains a diffusion——the source of minority carriers——and whose potential can be controlled, and an input gate that can be turned on and off to control the flow of charge from the source diffusion into the first potential well.

(2) The transfer section, containing a series of electrodes which control the potential at the Si-SiO2 interface. When the voltages on the electrodes are properly manipulated, the potential wells are moved toward the output, and the charge packets follow.

(3) The output section is a reverse biased *p-n* junction capacitance whose voltage is changed when a charge packet is transferred into it. The diode is then reset via a reset switch to prepare for the

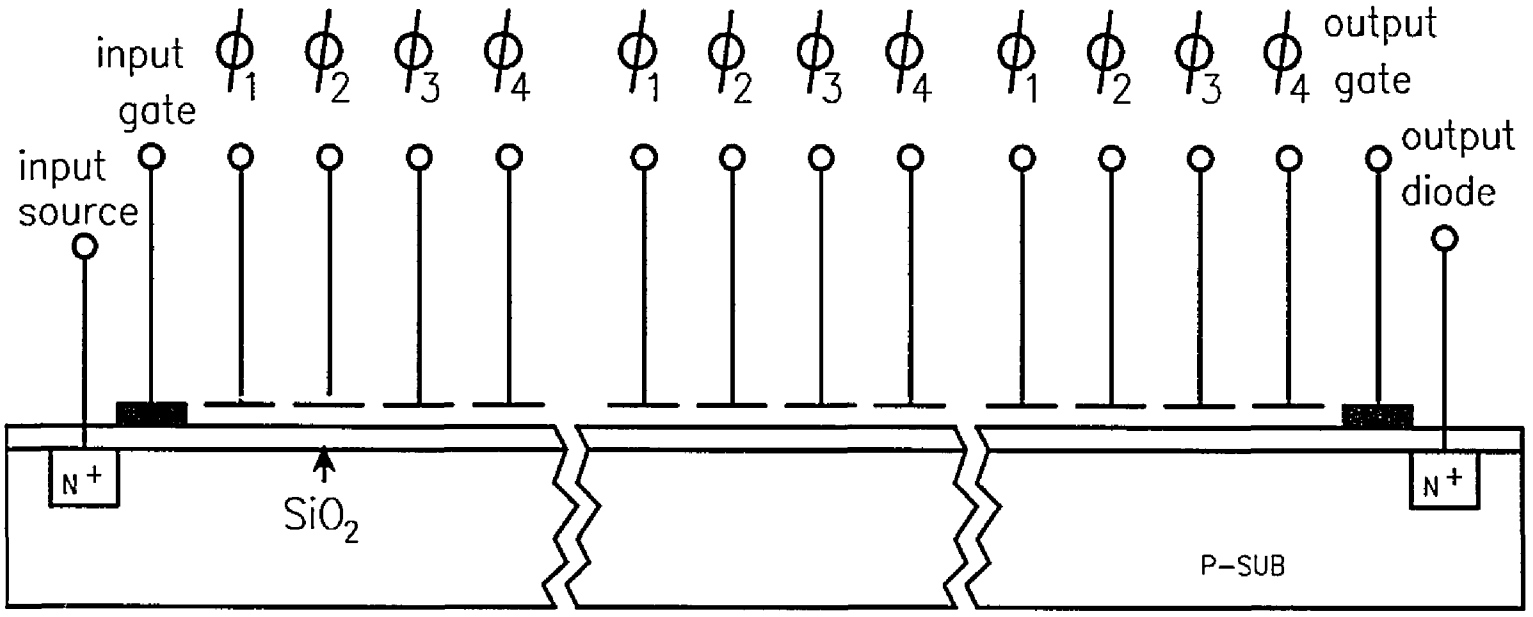

Fig. 3-1 Charge-coupled device

next packet to be transferred into it. This node is typically connected to a MOS amplifier.

3-2 Floating-Diffusion Amplifier

The floating diffusion amplifier (FDA) is the most popular approach for detecting the output signal with an on-chip amplifier. The on-chip preamplifier is shown in Fig. 3-2. The floating diffusion is periodically reset to the drain voltage, V_{REF}. Then, before each signal charge packet is introduced into the floating diffusion, the floating diffusion is isolated from the drain by the reset gate ϕ_{RESET}. To detect the output signal, the floating diffusion is connected to the gate of an on-chip MOS amplifier. The detected signal at the gate of the MOS device V_{out} is

$$V_{out} = \frac{Q_{Sig}}{C_{FD}} \tag{3-1}$$

where C_{FD} is the total capacitance associated with the floating diffusion.

Fig. 3-3 shows the equivalent circuit of the reset MOS resistance R_{MOS} and the sense node capacitance C_{FD} with an initial charge Q_o and corresponding V_o. At $t = 0$, a noiseless ideal switch is closed, charging the capacitor to the voltage V_{REF} through the MOS resistance R_{MOS}. It can be shown[5] that the mean-square deviation of the voltage

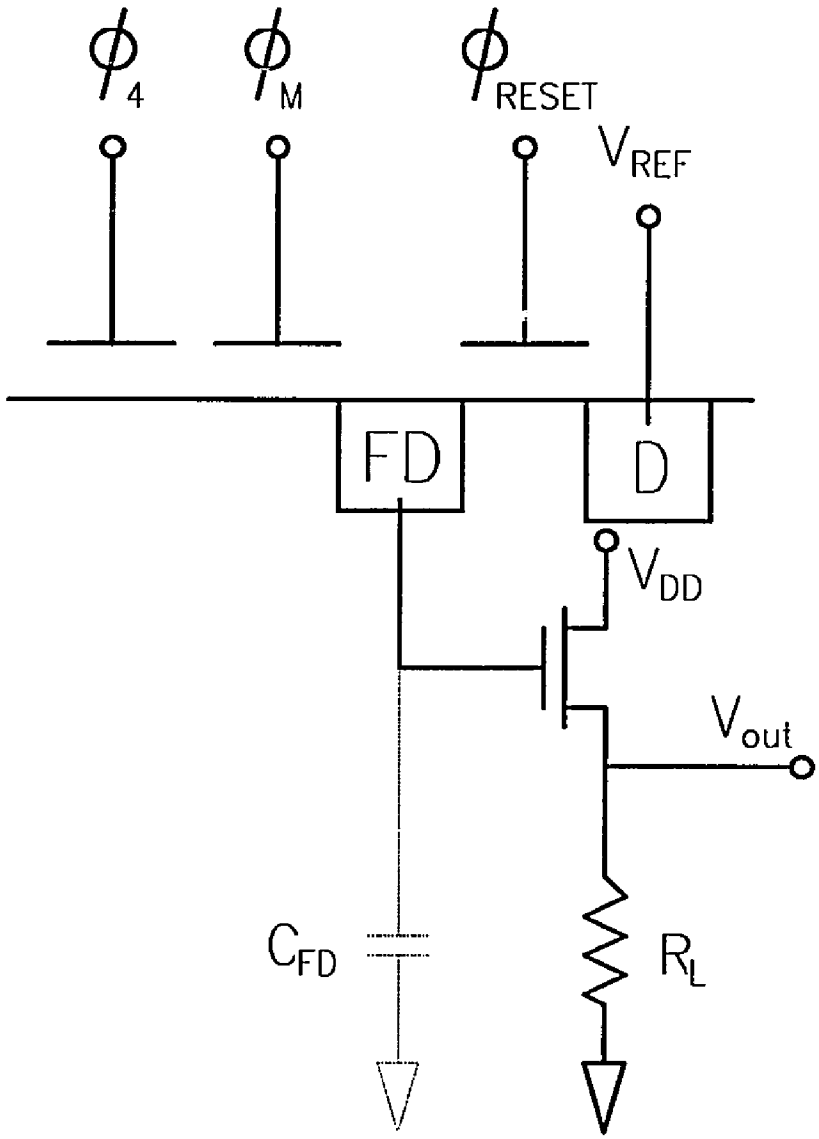

Fig. 3–2 Floating diffusion amplifier.

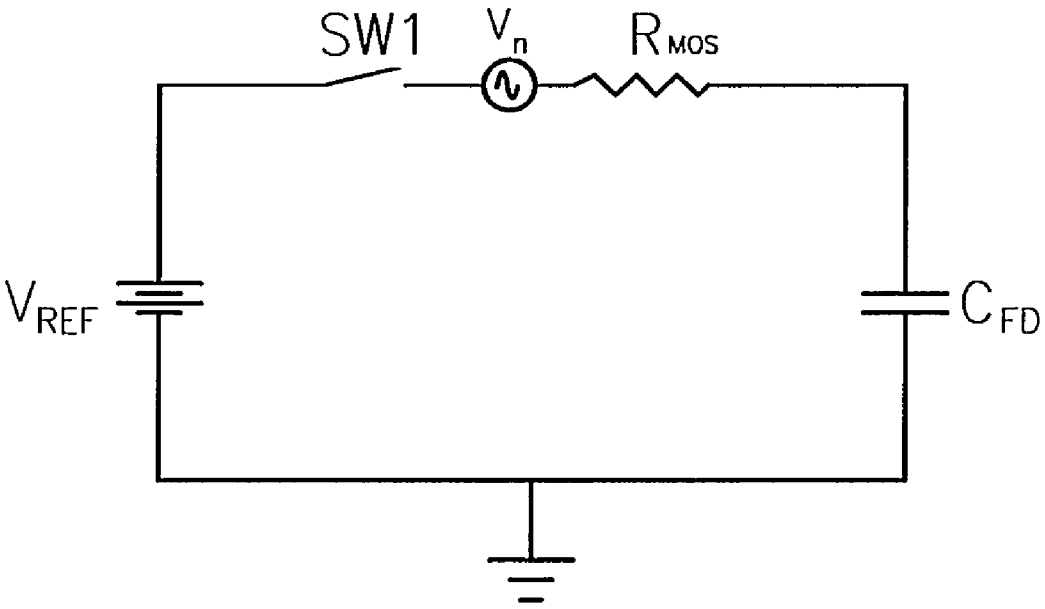

Fig. 3–3 Noise–equivalent circuit for the charging of a capacitor through a resistor having thermal noise.

across C_{FD} is given by

$$\overline{V^2(t)} = \frac{kT}{C_{FD}} [1-\exp(-2t/R_{MOS}C_{FD})] \qquad (3\text{-}2)$$

where k is the Boltzmann's constant and T is temperature. The complete charging curve is shown in Fig. 3-4.

Now consider the conventional CCD output circuit in Fig. 3-2. The readout sequences is as follows. The output diode (floating diffusion) is reset to some large reverse-bias voltage, V_{REF}, through a MOS switch. The time constant of the resetting of the output capacitance, which is given by $R_{MOS}(on)\cdot C_{FD}$, is typically $10^4\ \Omega\cdot 10^{-13}$ F = 10^{-9} sec. Thus dc-wise and noise-wise, the circuit will have reached its equilibrium state in a typical reset time 10^{-8} to 10^{-7} sec after the reset MOS has been turned ON. As the reset MOS is switched OFF, there will be a drop in the voltage waveform across C_{FD} due to reset clock feedthrough in the reset transistor (see Fig. 3-5); there will also be a longer delay having a time constant $R_{MOS}(off)\cdot C_{FD}$, which is typically $10^{12}\ \Omega\cdot 10^{-13}$ F = 10^{-1}sec. Next, the charge packet is clocked into the output diode, reducing its reverse bias. Typically, the voltage is sampled at instant B with respect to some fixed reference; in this case the r.m.s. noise voltage $(kT/C)^{1/2}$ present on the output waveform during the resetting determines the potential on the diode following the arrival of the signal charge packet, i.e., this noise is effectively present in the waveform at instant B. However, if two samples are taken, one at A just after the reset MOS is turned off and

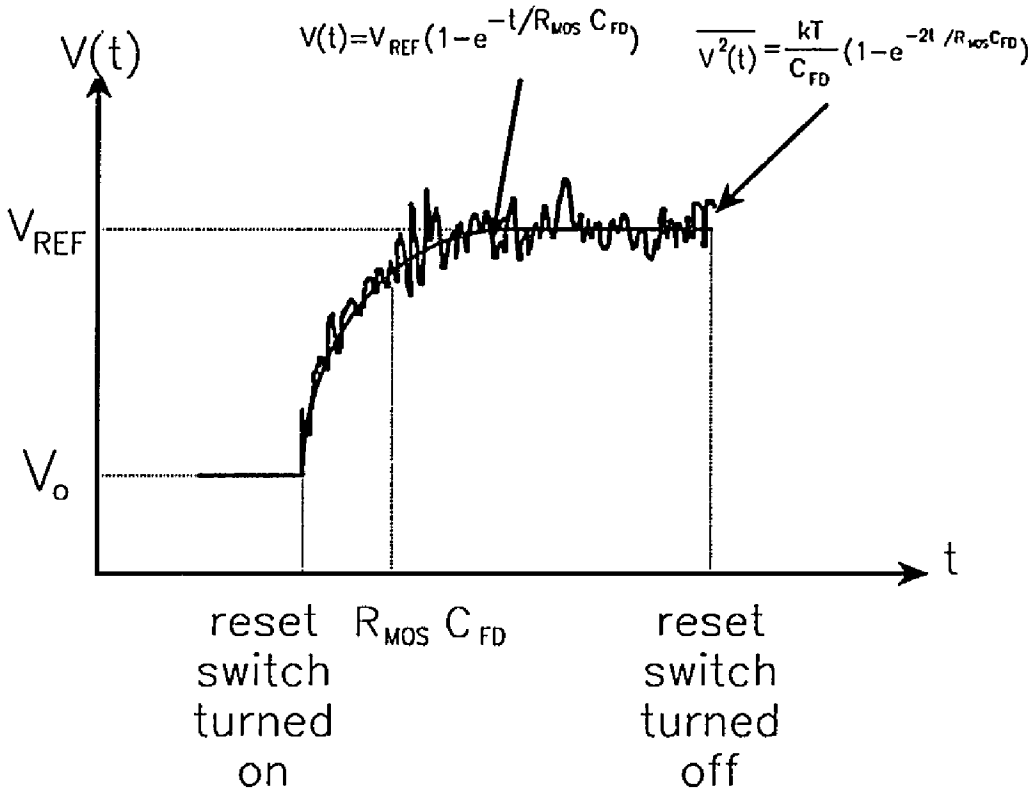

Fig. 3–4 Curves of mean voltage and noise voltage across a capacitor as a function of time.

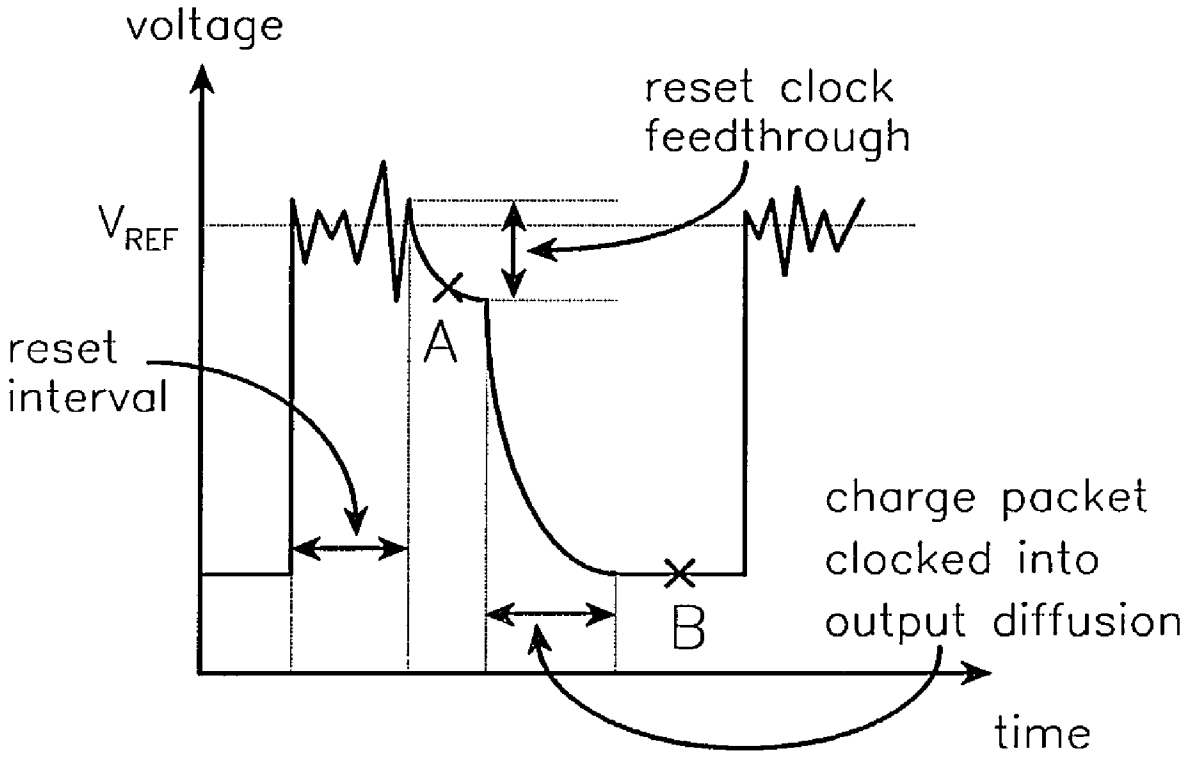

Fig. 3–5 output voltage waveform of reset amplifier output circuit, showing sampling points A and B.

the other at B after the signal charge has been clocked into the output diode, and if the time between A and B is much less than $R_{MOS}(off) \cdot C_{FD}$, then the noise on these samples is correlated and can be removed by subtracting V_A from V_B. This process is called correlated double sampling. The subtraction process is achieved by inverting and storing the reset voltage (at A) for subsequent comparison with the signal voltage (at B).

3-3 Correlated Double Sampling

The correlated double sampling (CDS) technique was first developed by M. White et. al.[6] for low light level image arrays. This technique not only has the capability, if properly implemented, to achieve very low noise levels but also has the additional advantages of being linear, stable and that implementation can be easily performed off chip (or on-chip) with only a few MOS transistors.

Fig. 3-6(a) is a schematic presentation of the circuit which was used to implement CDS. The portion of this circuitry which was on the CCD chip is composed of two MOSFETS, (shown in Fig. 3-6(a) as a switch and MOSFET), M_1 and M_2. The purpose of transistor M_1 (shown as a switch) is to preset the output capacitance C_{FD} (the capacitance of node A) to a reference voltage V_{REF}. The signal packet is then

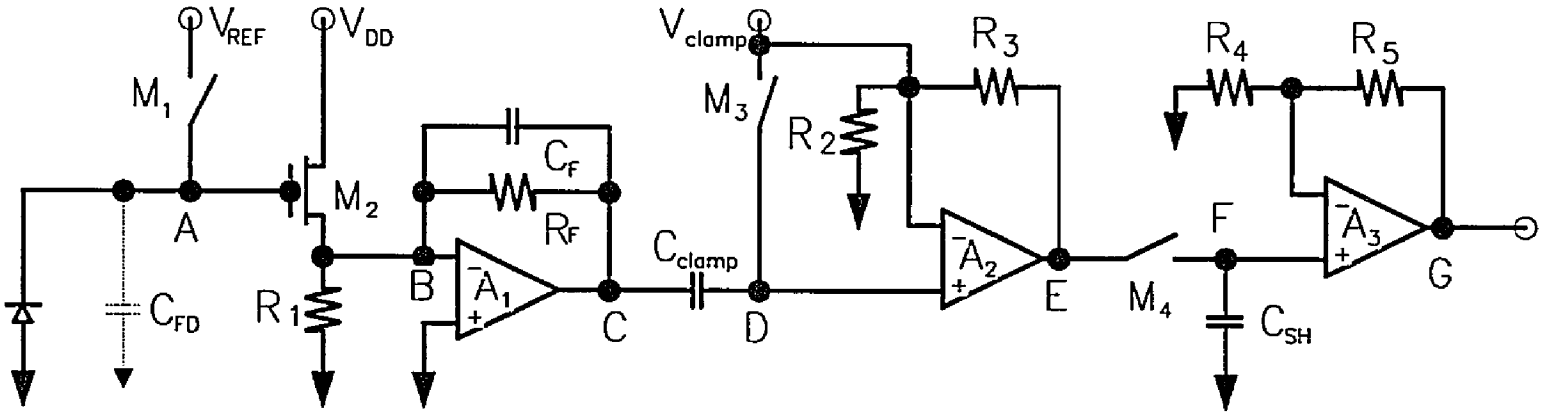

Fig. 3–6(a) Schematic diagram of a CDS processor.

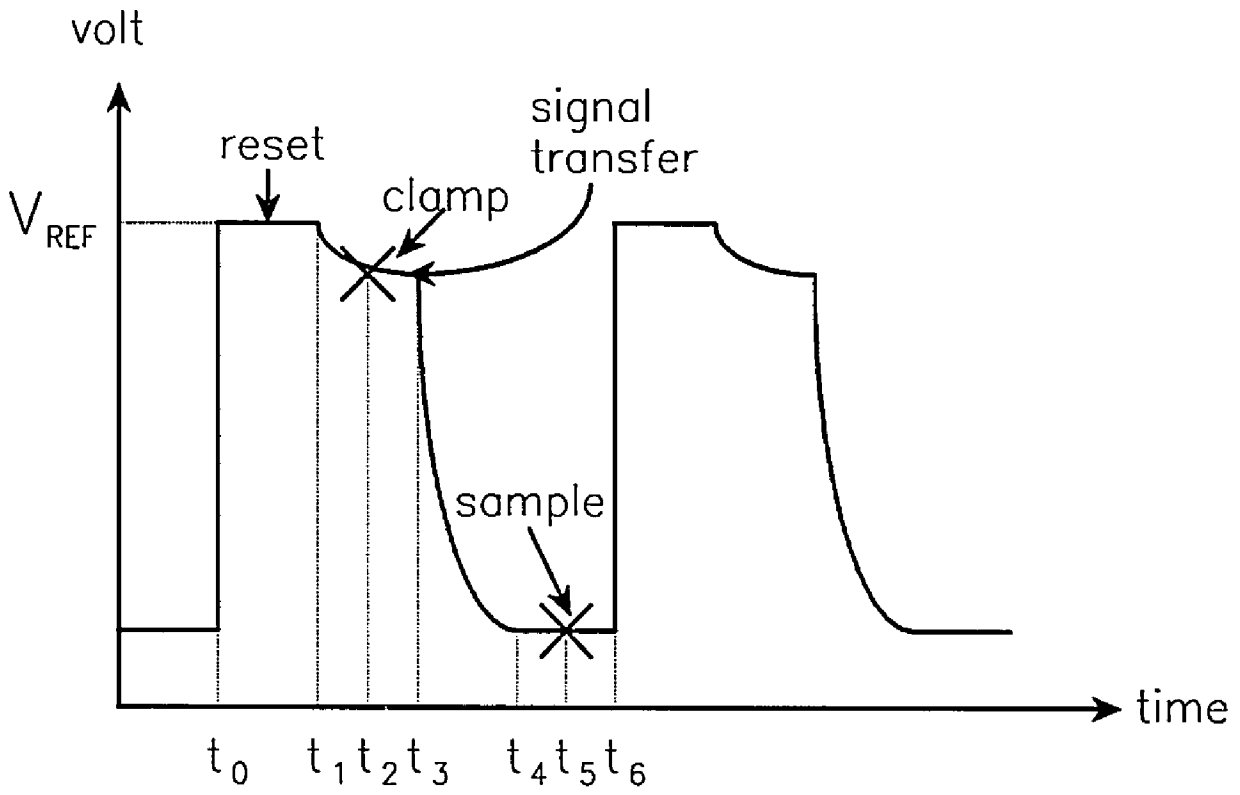

Fig. 3–6(b) Voltage waveform observed at point B in (a).

transferred onto this capacitor and discharges it towards ground. The resultant change in voltage is sensed by the source follower amplifier M2 and is brought off the chip at point B. The voltage waveform which is observed at point B is shown in Fig. 3-6(b). The four distinct timing subintervals employed in the readout circuit of Fig. 3-6 can be described as following:

(1) Reset interval ($t_0 \sim t_1$): Close and then open the reset switch M1. Node A is reset to the reference voltage V_{REF} with a noise uncertainty $(\overline{V_n^2})^{1/2}$. This noise voltage may be introduced through inadequate filtering of the reference supply voltage and the Nyquist noise contribution of the reset switch M1, where the latter is given by[1] $(\overline{V_n^2})^{1/2}=(kT/C_{FD})^{1/2}$. The full Nyquist voltage appears across C_{FD} when $R_{MOS}(on)\cdot C_{FD} \ll (t_1-t_0)$. At the start of the reset interval (time t_0) the pixel charge is in transit to the last well of the electrical bit (ϕ_4 in Fig. 3-2) adjacent to the transfer gate ϕ_M and the collection diode (see Fig.3-2).

(2) Read reset interval ($t_1 \sim t_3$): Close and then open the clamp switch M3 at time t_2. This procedure charges the clamp capacitor, C_{clamp}, to a voltage indicative of the voltage on the gate of the source follower M2, which is (V_{REF} + V_n). With the clamp switch off, the measured reset noise is holding on the high impedance node D formed by C_{clamp} and the input impedance of the buffer amplifier A2.

(3) Minority carrier signal input interval ($t_3 \sim t_4$): Cycle the transfer gate voltage ϕ_M to transfer a charge packet to the collection diode. The voltage on the circuit node A during this subinterval is

$$V_{sig} + V_{REF} + V_n$$

where V_{sig} is the signal voltage.

(4) Read signal interval ($t_4 \sim t_6$): Close and then open the sample and hold switch M4 to hold the signal at the output of the buffer amplifier A2. After the transfer gate (ϕ_M) is turned off, the output voltage across capacitor C_{clamp} consists of a time correlated difference signal between the input signal plus the reset level and the reset level due to the fact that the clamp switch M3 is now in the open state. Since there is negligible leakage of the reset level at circuit node A due to the long discharge time constant $R_{MOS(off)} \cdot C_{FD}$, the reset noise is correlated within a pixel time window. Thus the voltage appearing across the clamp capacitance, C_{clamp}, is a measure of the time difference between the signal plus the reset level minus the reset level, i.e.,

$$[V_{sig} + V_{REF} + V_n] - [V_{REF} + V_n] = V_{sig} \qquad (3\text{-}3)$$

The signal increment is amplified and passed to the output of the signal processor by the closure of the sample switch M4.

What is significant about the operation of CDS is that the sampled noise, i.e., the Nyquist voltage uncertainty at the "read reset" time is correlated to that sampled at the "read signal" time. The time correlation method provides the removal of Nyquist noise in the reset MOSFET switch.

3-4 Simulation of CCD Output Circuit

A laboratory model has been made as shown in Fig. 3-7 to simulate the operation of a CCD output circuit. In Fig. 3-7, capacitor C_1 is used to simulate the last potential well in a CCD array. Before the readout takes place, C_1 is charged to a signal voltage V_{sig} through switch J_1. Thus, a charge packet $Q_{sig} = V_{sig} \cdot C_1$ is stored in the storage capacitance C_1 prior to the transfer gate J_2 being turned on. Diode D_1 works as the collection diode (floating diffusion) and capacitor C_2 presents the total capacitance associated with the floating diffusion in a CCD array. Operational amplifier A_1 with resistors $R_1 \sim R_4$ forms a unit-gain summer and operational amplifier A_2 in association with resistors $R_5 \sim R_7$ gives the function of a unit-gain inverter. Hence, what appears at the output of the operational amplifier A_2 is the sum of a reference level V_{REF} and a calibrated noise which is introduced by a Hp 3722A noise generator. Switch S_1 provides the option of whether to have the noise present to simulate

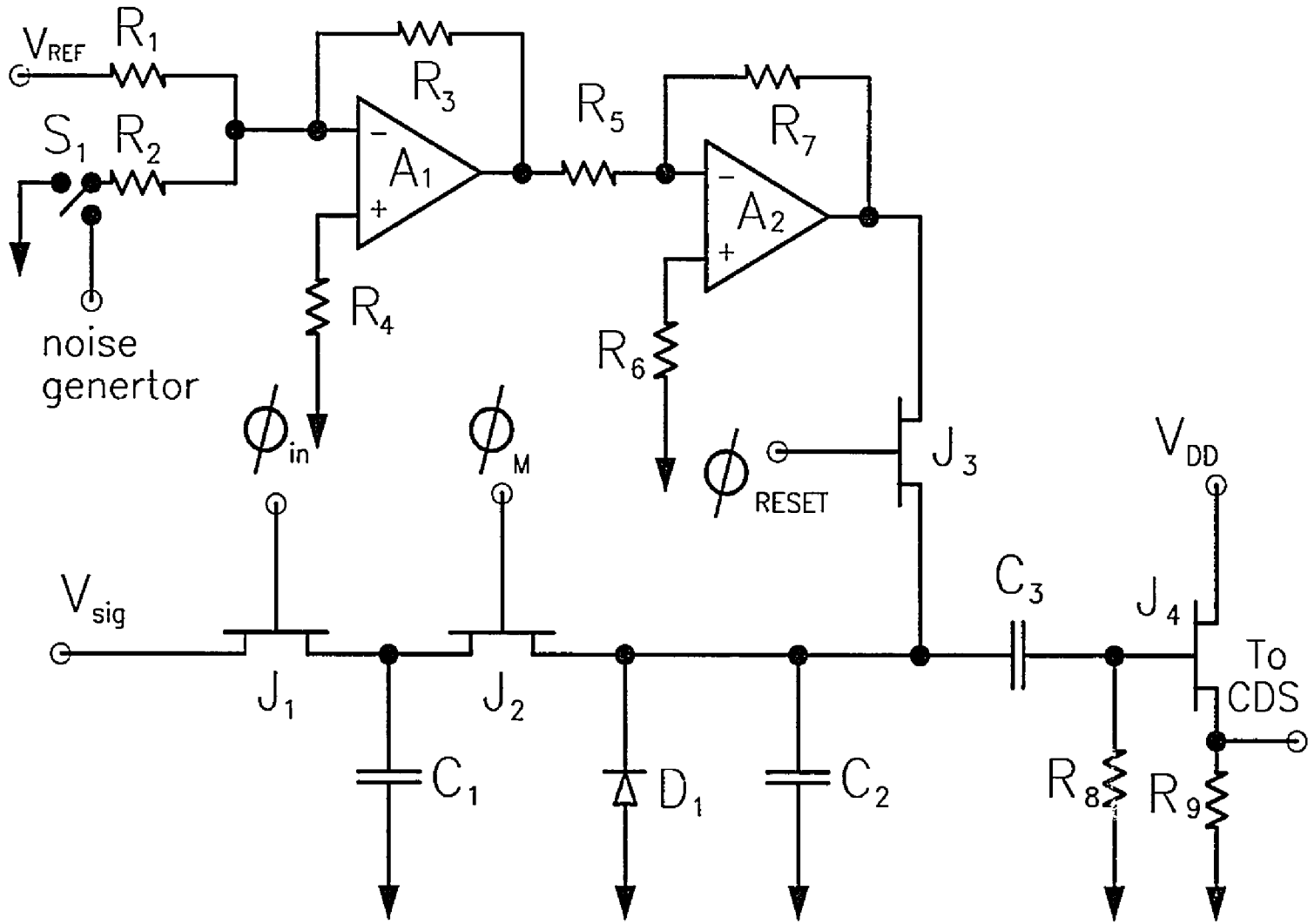

Fig. 3—7 Schematic diagram of CCD readout simulation circuit.

the reset noise or not. Transistor J3 has the same function as a reset switch by means of controlling gate voltage ϕ_{RESET}. The combination of transistor J4, capacitor C_3 and resistors R8 ~ R9 is a source follower, and the voltage taken from the source of transistor J4 is sent to CDS for further processing. In the source follower transistor, J4 is self-biased using a source resistance R9 and the resistance R8 provides dc continuity for the gate terminal.

The timing diagram for operating the simulation model is shown in Fig. 3-8. A signal charge packet Q_{sig} is generated by charging capacitance C_1 via switch J1. Note that when switch J1 is on, switch J2 is turned off (see Fig. 3-8), thus capacitor C_1 is isolated from the rest of the circuit. During time interval t_0 to t_1, capacitance C_1 is charged to a voltage V_{sig}. If C_1 = 500 pF and R_{on} = 50 Ω then the charge time constant will be 25 nsec. Hence, a charging time interval (when switch J1 is on) of 1 μsec will be sufficient to charge C_1 to V_{sig}. Meanwhile, capacitor C_2 is charged to the reference level V_{REF} (or V_{REF} + noise if switch S1 is closed) through switch J3. At time t_2 a clamp switch in the CDS circuit is turned on to sample and hold the reference level (plus noise). During the "minority carrier signal input" interval (t_3 ~ t_4) switches J1 and J3 are turned off and switch J2 is turned on, capacitance C_2 is charged to a level equal to $V_{sig}\cdot[C_1/(C_1+C_2)]$. After switch J2 being turned off at t_4, capacitance C_2 will hold a charge packet of $Q'_{sig} = V_{sig}\cdot[C_1/(C_1+C_2)]\cdot C_2$. One can

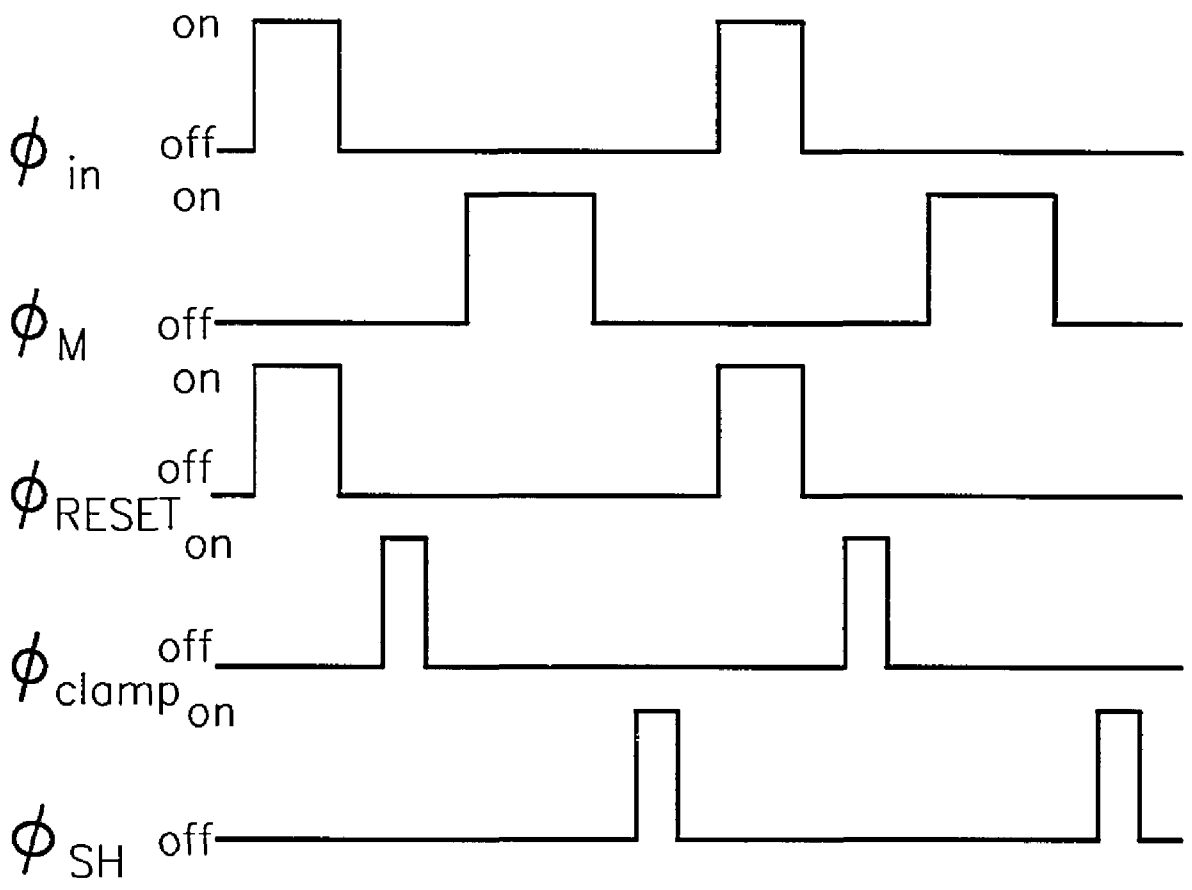

Fig. 3-8 Timing diagram of CDS operation.

assume that in a real CCD array, the charge transferred to the collection diode is just Q_{sig}. For simplicity, Q_{sig} will be used instead of Q'_{sig}. Switch ϕ_{SH} in the CDS circuit is turned on and then off at time t_S to complete one cycle of the signal readout, i.e., read out one pixel.

Recall that the Nyquist noise contribution of the reset switch J_3 has an r.m.s. value given by $(kT/C_2)^{1/2}$. In the simulator, C_2 has a value of 100 pF which is much greater than C_{FD} = 0.1 pF in a typical CCD array and therefore the reset noise introduced onto capacitance C_2 in the simulative circuit is very small. To evidence the removal of the reset noise, the Hp 3722A noise generator is connected to one of the summer's terminals to introduce simulated reset noise at a visible level.

3-5 Experiment Setup

A block diagram of the experiment setup is provided in Fig. 3-9. Most of the equipment shown is from the CCD Array Test Facility which is located in the Optical Detection Lab at the Optical Sciences Center.

The CCD Array Test Facility is a set of programmable hardware modules interfaced to a controlling microcomputer. The instrument

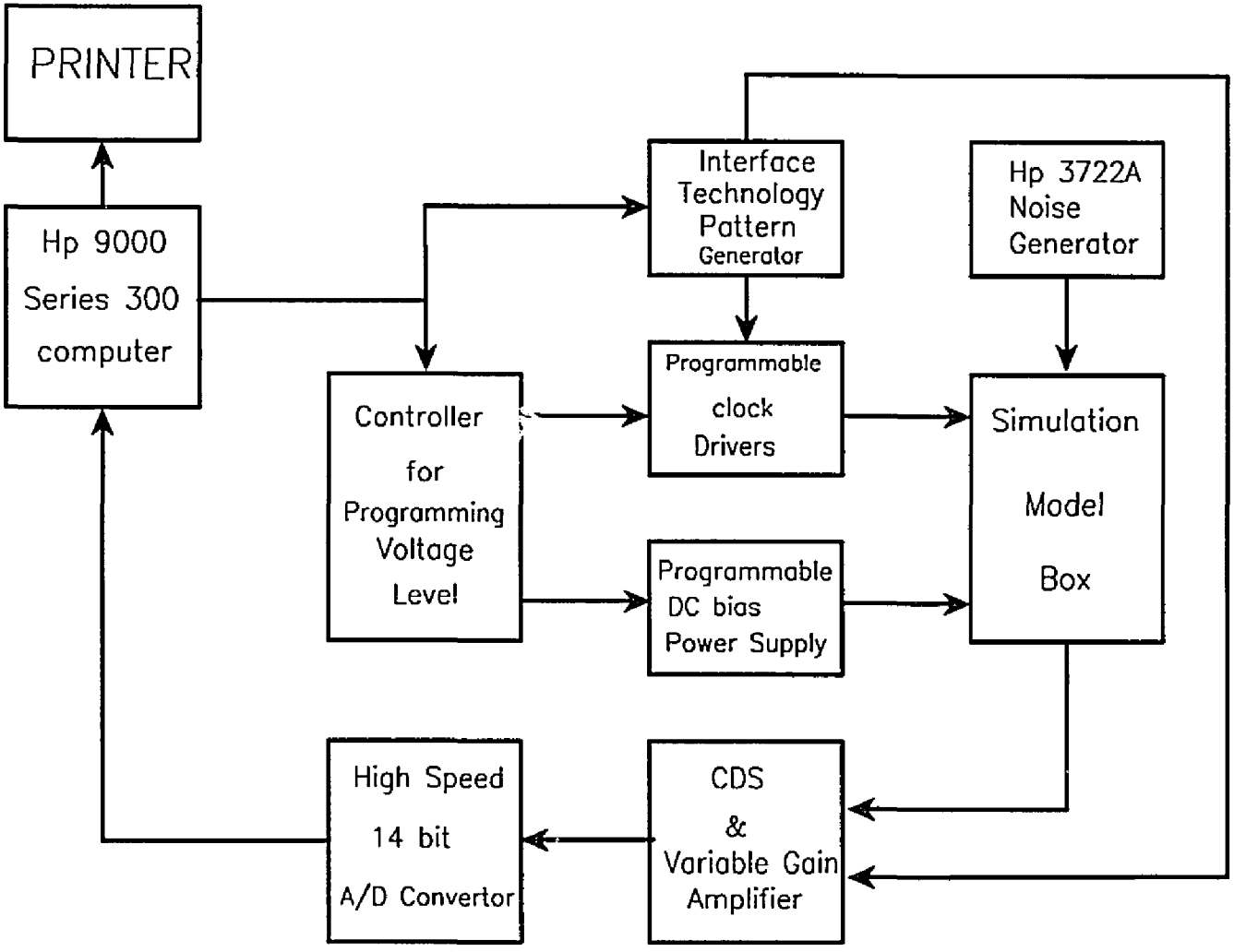

Fig. 3-9 Experiment setup.

control computer is a Hewlett-Packard Hp 9000 Series 300 computer. The Hp 9000 Series 300 computer communicates with the test rack instrumentation modules over the HPIB or IEEE 488 bus. The test rack instrumentation consists of the following:

(1) a Pulse Instruments PI-952 interface unit.

(2) a Tustin 14-bit high-speed A/D converter unit with correlated double sampling modification.

(3) an Interface Technology RS-432 programmable pattern generator.

(4) 18 Pulse Instruments PI-451 programmable pulse drivers.

(5) 6 Pulse Instruments PI-702 programmable dual bipolar DC voltage source modules.

The equipment necessary to operate the simulation model includes the pattern generator and clock drivers. These devices produce the waveforms that are needed to switch transistors J_1 ~ J_3 on and off in an orderly manner. The microcomputer is used to process the different timing sequences for different tests. The signal from the output of the simulation model is sent to the CDS circuit which is combined with a variable gain amplifier installed inside the Tustin A/D converter. The A/D converter converts each pixel signal into a digital signal that is stored in the Hp 9000 Series 300 computer for future noise spectrum estimation. A Hewlett-Packard Hp 3722A noise generator is also employed to introduce band-limited white noise with calibrated characteristics.

3-6 Spectrum Analysis

Estimation of the power spectral density (PSD) function, or simply the spectrum, of discretely sampled deterministic and stochastic processes is usually based on procedures employing the fast Fourier transform (FFT). This approach to spectrum analysis is computationally efficient and produces reasonable results for a large class of signal processes. In spite of these advantages, there are several inherent performance limitations of the FFT approach. The most prominent limitation is that of frequency resolution, i.e., the ability to distinguish the spectral responses of two or more signals. The frequency resolution in hertz is roughly the reciprocal of the time interval in seconds over which sampled data is available. A second limitation is due to the implicit windowing of the data that occurs when processing with the FFT. Windowing manifests itself as "leakage" in the frequency domain, i.e., energy in the main lobe of a spectral response "leaks" into the sidelobes, obscuring and distorting other spectral characteristics that are present. Skillful selection of tapered data windows can reduce the effects of spectral leakage, but always at the expense of reduced resolution. These two performance limitations of the FFT approach are particularly troublesome when analyzing short data records. In an attempt to alleviate the inherent limitations of the FFT approach, many alternative spectral estimation procedures have been proposed within the last decade.

Windowing of data makes the implicit assumption that the unobserved data values outside the window are zero, which is normally an unrealistic assumption. Often, one has more knowledge about the process from which the data samples are taken, or at least is able to make a more reasonable assumption other than to assume the data is zero outside the window. Use of a priori information (or assumptions) may permit selection of an exact model for the process that generated the data samples, or at least a model that is a good approximation to the actual underlying process. It is then usually possible to obtain a better spectral estimate based on the model by determining the parameters of the model from the observations.

3-7 Autoregressive Spectrum Analysis Algorithm

Autoregressive (AR) spectrum analysis has become a popular alternative to the conventional FFT approach for estimating the power spectral density of a sampled process. For example, a data set sampled by correlated double sampling can be a good candidate for using AR spectral estimation. Autoregressive spectral estimates do not have the distortion produced by sidelobe leakage effects that are inherent in the FFT approach to spectrum analysis.

The method used to estimate the autoregressive model parameters is the key to the performance of the AR technique. If M+1 lags of the autocorrelation function for a process are known, the M autoregressive parameters can be obtained by solving the Yule-Walker normal equations using the Levinson recursion algorithm[7].

If an autoregression is a reasonable model for the data, then the observed sequence $\{x_n\}$ is the output from a pth order AR model driven by a white noise sequence $\{w_n\}$ of zero mean and variance σ^2. Mathematically, the output sample x_n is a weighted sum of p past output samples plus a noise term:

$$x_n = -\sum_{k=1}^{p} a_k \cdot x_{n-k} + w_n. \tag{3-4}$$

where a_k is an AR parameter of the pth order AR process.

To estimate the PSD, a relationship, known as the Yule-Walker equations, between the AR parameters and the autocorrelation function (known or estimated) of x_n may be written as[7]:

$$R_{xx}(k) = \begin{cases} -\sum_{\ell=1}^{p} a_\ell R_{xx}(k-\ell), & \text{for } k > 0 \\ -\sum_{\ell=1}^{p} a_\ell R_{xx}(-\ell) + \sigma^2, & \text{for } k = 0. \end{cases} \tag{3-5}$$

The output power spectral density $S_x(f)$ is related to the input noise power spectral density $S(f) = \sigma^2 \Delta t$ by

$$S_x(f) = \frac{\sigma^2 \Delta t}{\left| 1 + \sum_{k=1}^{p} a_k \cdot \exp(-j2\pi f k \Delta t) \right|^2} \tag{3-6}$$

where Δt is the autocorrelation lag interval in seconds. Thus, to estimate the PSD, one need only estimate $\{a_1, a_2, \ldots, a_p, \sigma^2\}$. To determine the AR parameters, one can choose p equations from eq. (3-5) for $k > 0$, solve for $\{a_1, a_2, \ldots, a_p\}$, and then find σ^2 from eq. (3-5) for $k = 0$, i.e.,

$$\sigma^2 = Rxx(0) + \sum_{\ell=1}^{p} a_\ell Rxx(-\ell). \tag{3-7}$$

The Levinson algorithm provides an efficient solution to eq. (3-5). The algorithm proceeds recursively to compute the parameter sets $\{a_{11}, \sigma^2\}$, $\{a_{21}, a_{22}, \sigma^2\}, \ldots,$ $\{a_{p1}, a_{p2}, \ldots, a_{pp}, \sigma_p^2\}$. Note that an additional subscript has been added to the AR parameters to denote the order. The final set at order p is the desired solution. In particular, the recursive algorithm is initialized by

$$\begin{aligned} a_{11} &= -Rxx(1)/Rxx(0) \\ \sigma_1^2 &= (1-|a_{11}|^2)Rxx(0) \end{aligned} \tag{3-8}$$

with the recursion for $k = 2, 3, \ldots, p$ given by

$$a_{kk} = -[Rxx(k) + \sum_{\ell=1}^{k-1} a_{k-1,\ell} Rxx(k-\ell)]/\sigma_{k-1}^2$$

$$a_{ki} = a_{k-1,i} + a_{kk} \cdot a_{k-1,k-i}$$

$$\sigma_k^2 = (1-|a_{kk}|^2) \cdot \sigma_{k-1}^2 \quad .$$

Note that the Levinson algorithm also provides the AR parameters for all the lower order AR models.

A host of techniques are available for estimating the AR parameters from data samples. The most obvious approach is to first make estimates of the autocorrelation lags with the available data, and then apply the usual Levinson recursion using the estimated lags. Spectral line splitting and the shifting of spectral peaks from their true locations are the reasons that this approach is rarely used[7].

The most popular approach for AR spectral estimation is the Burg algorithm[7]. This algorithm utilizes a constrained least squares estimation procedure to obtain the M estimated autoregressive parameters from N data samples. The constraint requires the AR parameter estimates to satisfy the Levinson recursion. AR spectral estimates based on the Burg algorithm suffer from the two same problems——spectral line splitting and shifting of spectral peaks.

In 1980, a recursive algorithm was published by Marple[10] for AR parameter estimation , based on a least-squares solution for the AR parameters using forward and backward linear prediction. The AR spectra yielded by Marple's algorithm present no line splitting and reduced spectral peak shifting. Also, Marple's algorithm has comparable computational complexity to the popular Burg algorithm. It is Marple's least squares algorithm that has been adopted in this thesis work for AR parameter estimation.

CHAPTER IV DATA ANALYSIS

4-1 CALIBRATION BETWEEN NOISE GENERATOR AND MARPLE'S AR SPECTRUM ESTIMATION

As mentioned in the last chapter, the spectrum estimation strategy adopted for work is an autoregressive (AR) model using Marple's algorithm to determine its parameters. A computer program, MARPLE, coded in BASIC is used for handling data sampling and spectrum estimation. Before MARPLE became a reliable tool for handling spectrum estimation it was necessary to do some calibration.

For the purpose of calibrating MARPLE, an experimental arrangement is shown in Fig. 4-1. The Hp 3722A noise generator has a built-in lowpass filter with cutoff frequencies at 50 KHz, 15 KHz, 5 KHz, 1.5 KHz, 500 Hz, 150 Hz, etc. Another low-pass filter with variable cutoff frequency is also available when a cutoff frequency other than those provided by the noise generator is needed. According to the operation manual of the Hp 3722A noise generator, this equipment can produce Gaussian noise with a spectrum as shown in Fig. 4-2.

During the calibration, 16384 samples were taken at a sampling frequency of 250 KHz. Before the sampled data was used to calculate

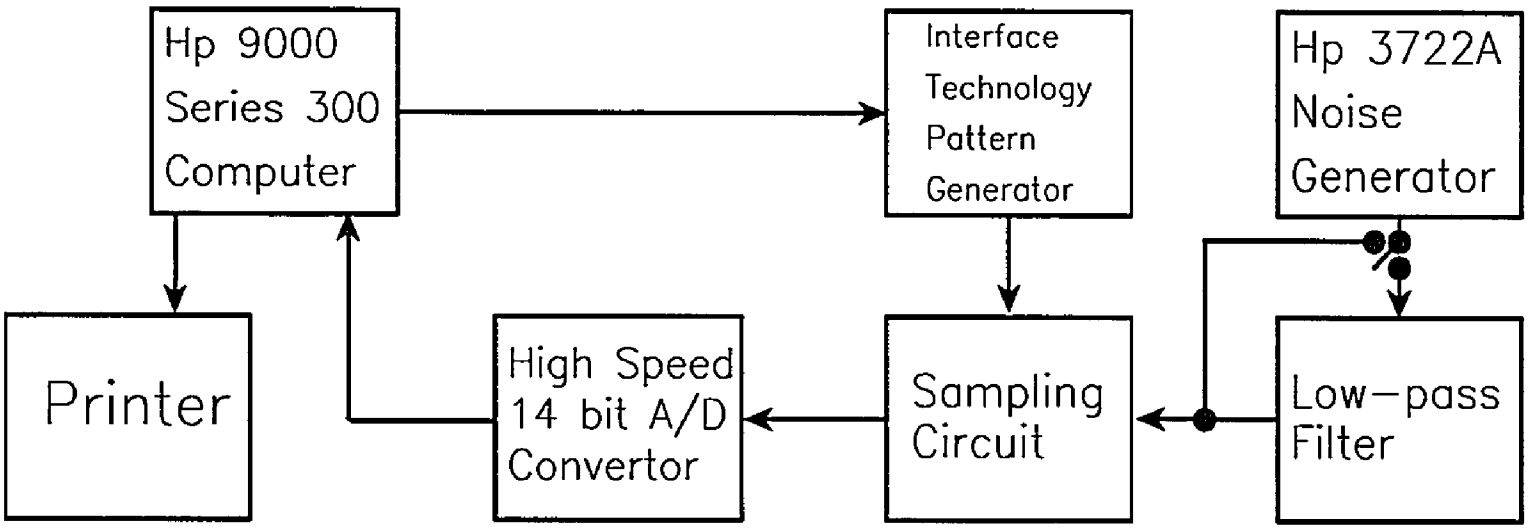

Fig. 4-1 Experimental setup for calibrating MARPLE.

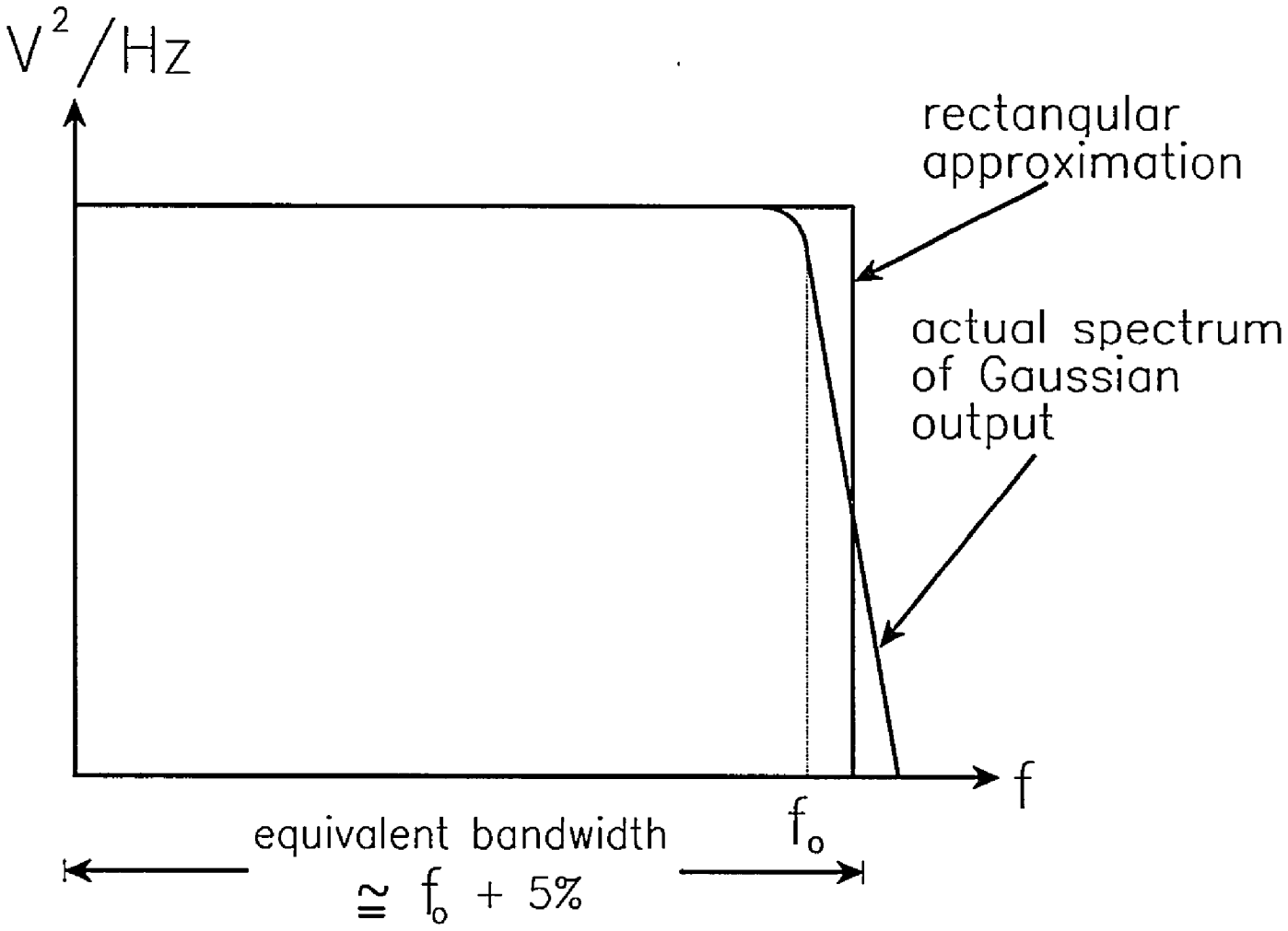

Fig. 4–2 Equivalent rectangular spectrum.

the AR parameters, the mean value of this set of data was subtracted from each sample in order to have a sequence of data with zero mean. Furthermore, the mean-square value, rms^2, of the zero-mean data samples was obtained by

$$rms^2 = \frac{1}{N}\sum_{i=1}^{N} x_i^2 \qquad (4\text{-}1)$$

where $x_1, x_2, \ldots, x_n$ are the N samples of the (zero mean) data. After processing this data using Marple's least squares algorithm, a plot of power spectral density versus frequency was generated. Twice the area beneath the power spectral density curve, which is the power delivered by the noise generator, is also calculated.

Fig. 4-3 illustrates the computer printouts of the power spectral density versus frequency. Curves in Fig. 4-3(a) and Fig. 4-3(b) show the spectrum of the noise after passing through a low-pass filter with cutoff frequencies of 5280 Hz and 10080 Hz, respectively. Together with these plots are the values of the mean-square and twice the area, which are very consistent. In Fig. 4-3(c) ~ (g), spectra were obtained for noise coming from the noise generator directly. The cutoff frequencies of the built-in lowpass filter were set at 50 KHz, 15 KHz, 5 KHz, 1.5 KHz, and 500 Hz, respectively. They also show good consistency between the mean-square value and power (twice the area beneath the curve). The shapes of those plots are approximately rectangular.

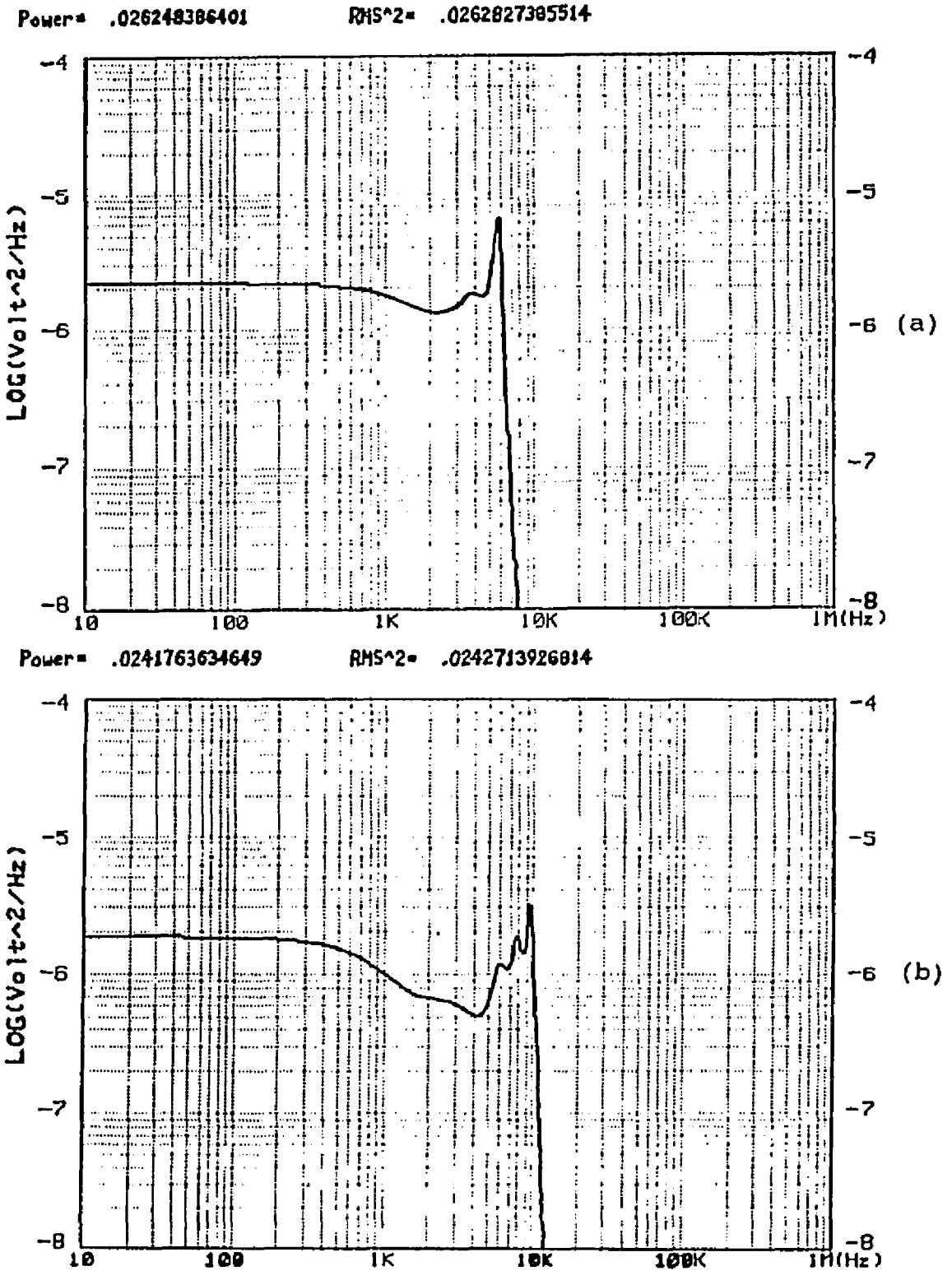

Fig. 4-3 Low-Pass Filtered Noise Power Spectral Density as a Function of f, f_c = (a)5280 Hz (b) 10080 Hz.

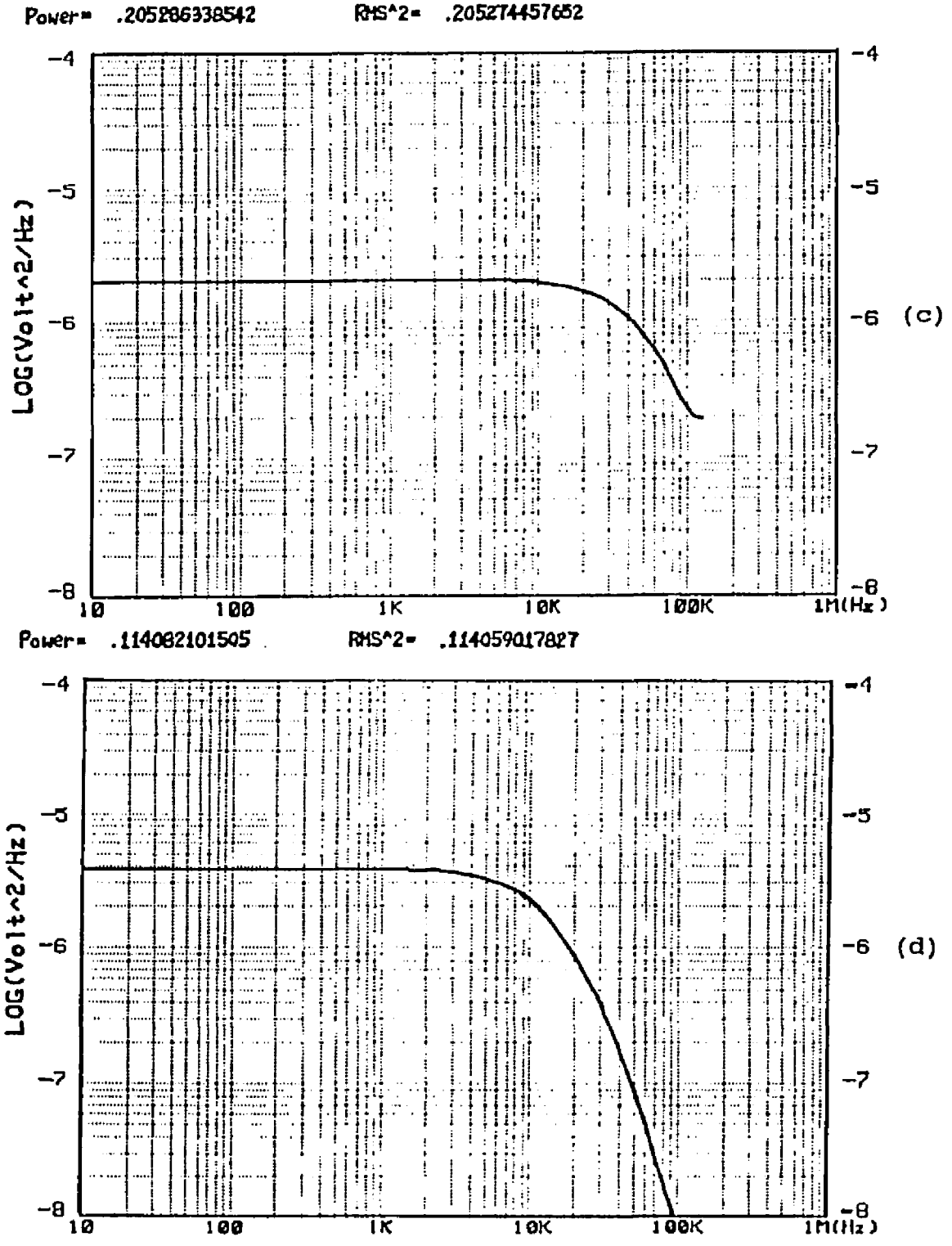

Fig. 4-3 Low-Pass Filtered Noise Power Spectral Density as a Function of f, f_c = (c) 50 kHz (d)15 kHz.

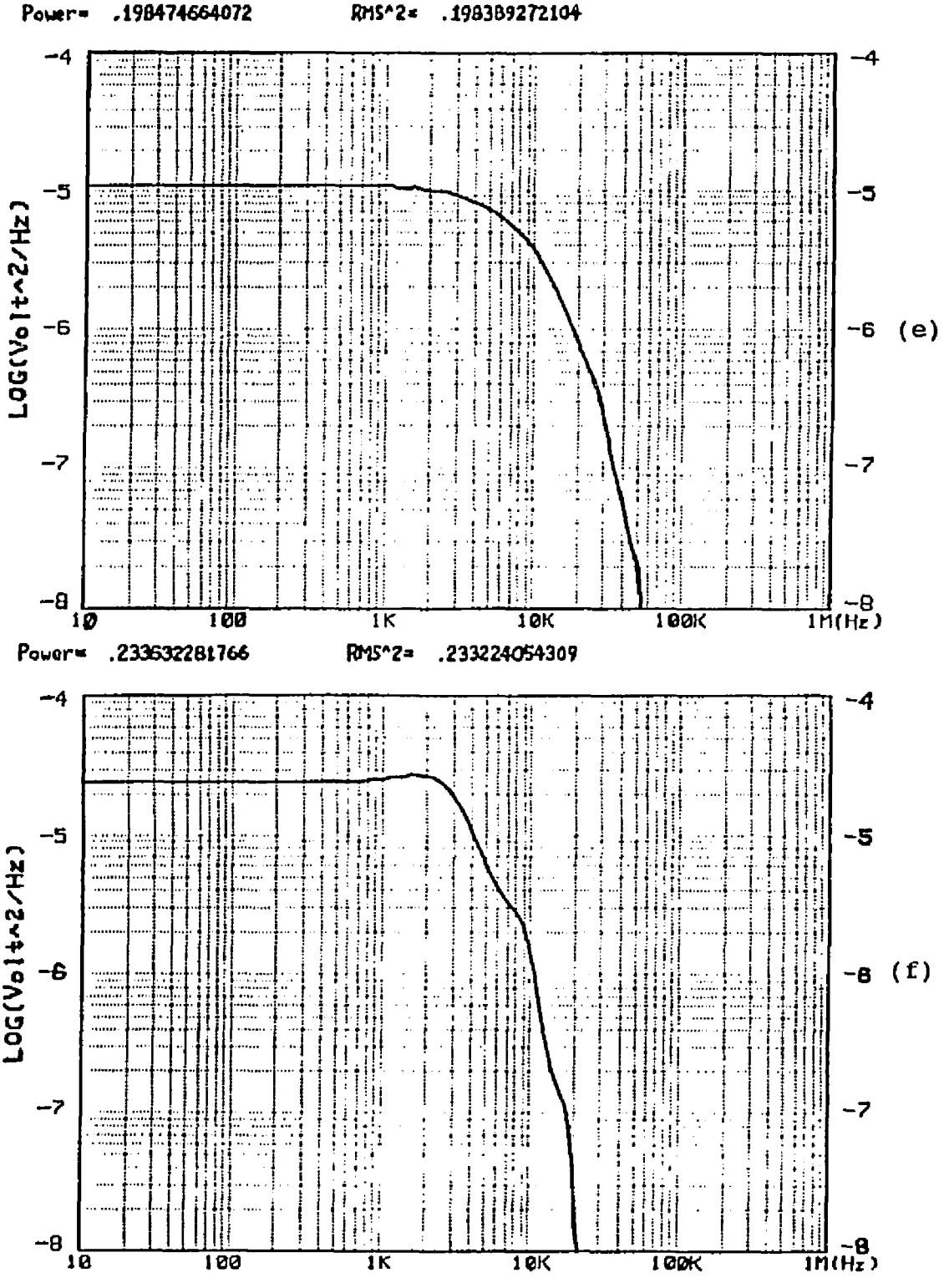

Fig. 4-3 Low-Pass Filtered Noise Power Spectral Density as a Function of f, f_c = (e) 5 kHz, (f) 1.5 kHz.

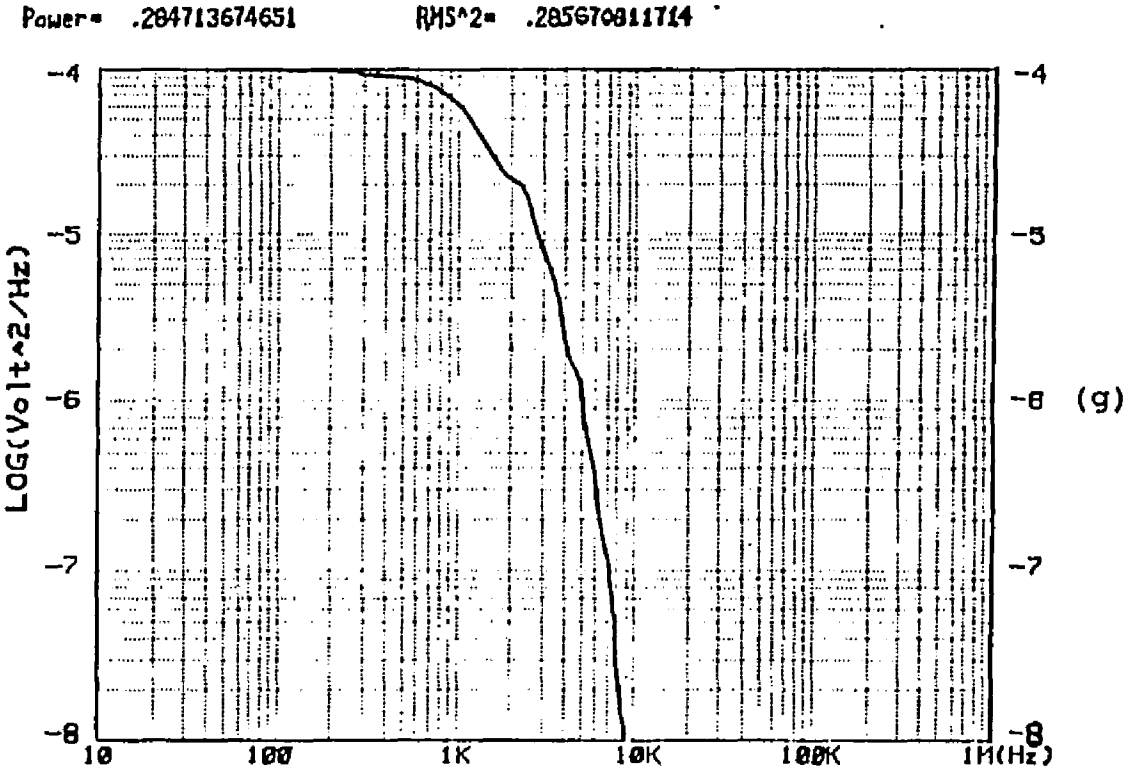

Fig. 4-3 Low-Pass Filtered Noise Power Spectral Density as a Function of f, f_c = (g) 500Hz.

Aliasing is observed when the sampling frequency f_s is not high enough. Fig. 4-4 shows the results of undersampling and oversampling. The cutoff frequency f_c of the band-limited white noise is set at 15 KHz and the sampling frequencies are adjusted to 250 KHz, 125 KHz, 62.5 KHz, 50 KHz, 25 KHz, 12.5 KHz, 6.25 KHz and 5 KHz. When the ratio f_s/f_c is decreased below two, the aliasing effect becomes pronounced.

4-2 Noise Reduction in Correlated Double Sampling

The goal of correlated double sampling (CDS) is to remove the reset noise introduced by the reset switch used in the CCD output stage. Theoretically, if the noise values at the time of "clamp" and "sampling" (t_2 and t_s in Fig. 3-6) are correlated, then the noise can be reduced by the correlated double sampling technique. The principle of CDS operation has been provided in Chapter 3. In this section, the experimental results are presented.

The experiments were performed in the Optical Detection Lab to show the noise reduction effect. The experimental arrangement is shown in Fig. 3-9. First of all, the power spectral density of the noise source alone, which is added to the reference level later in the experiment, is measured. Fig. 4-5(a) shows that the noise generator delivers band-limited white noise with bandwidth of 15 KHz. It also shows the power inside the band is approximately 0.087 V^2.

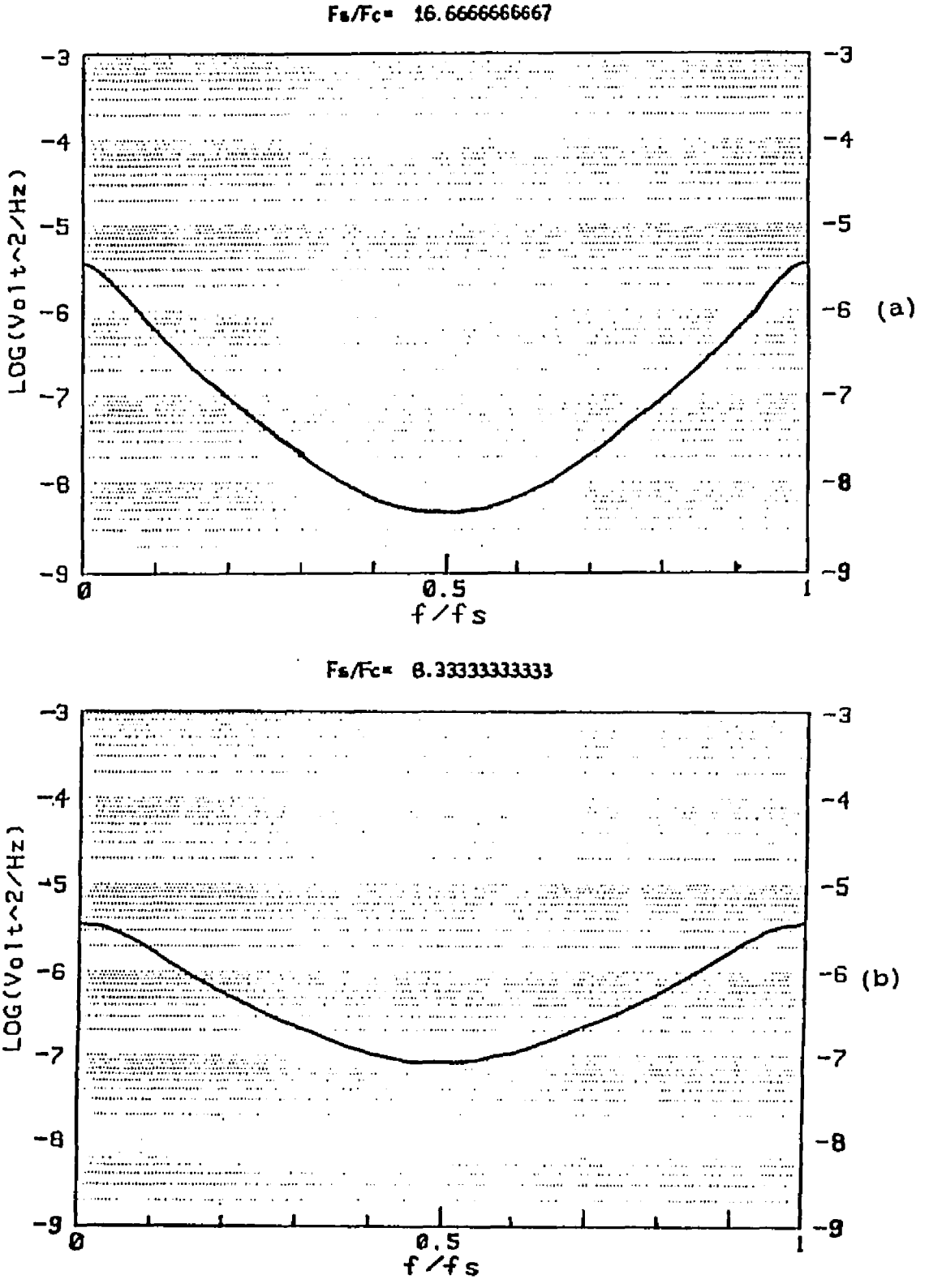

Fig. 4-4 Sampled Noise Spectrum with Different Ratios f_s/f_c

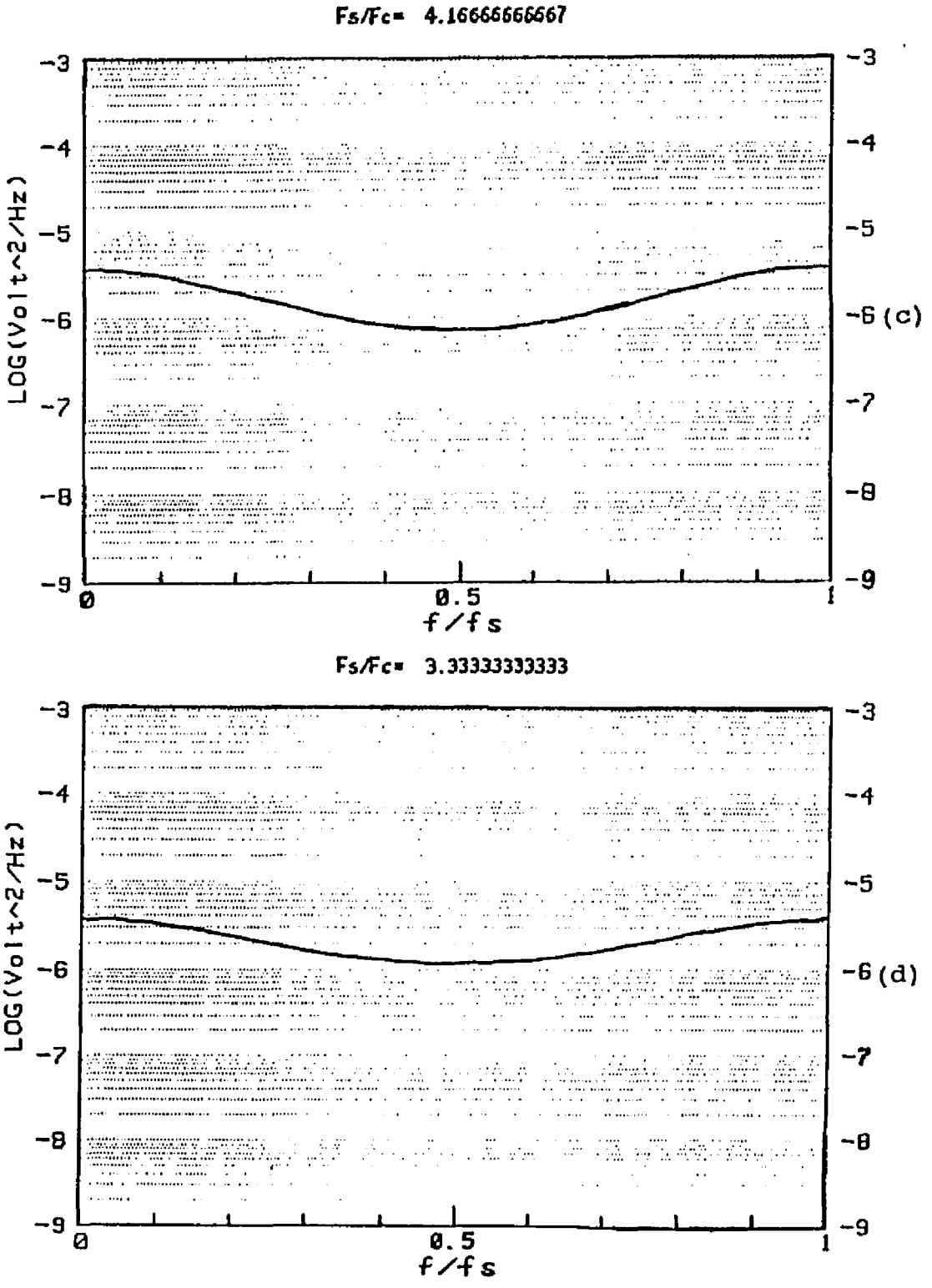

Fig. 4-4 Sampled Noise Spectrum with Different Ratios f_s/f_c

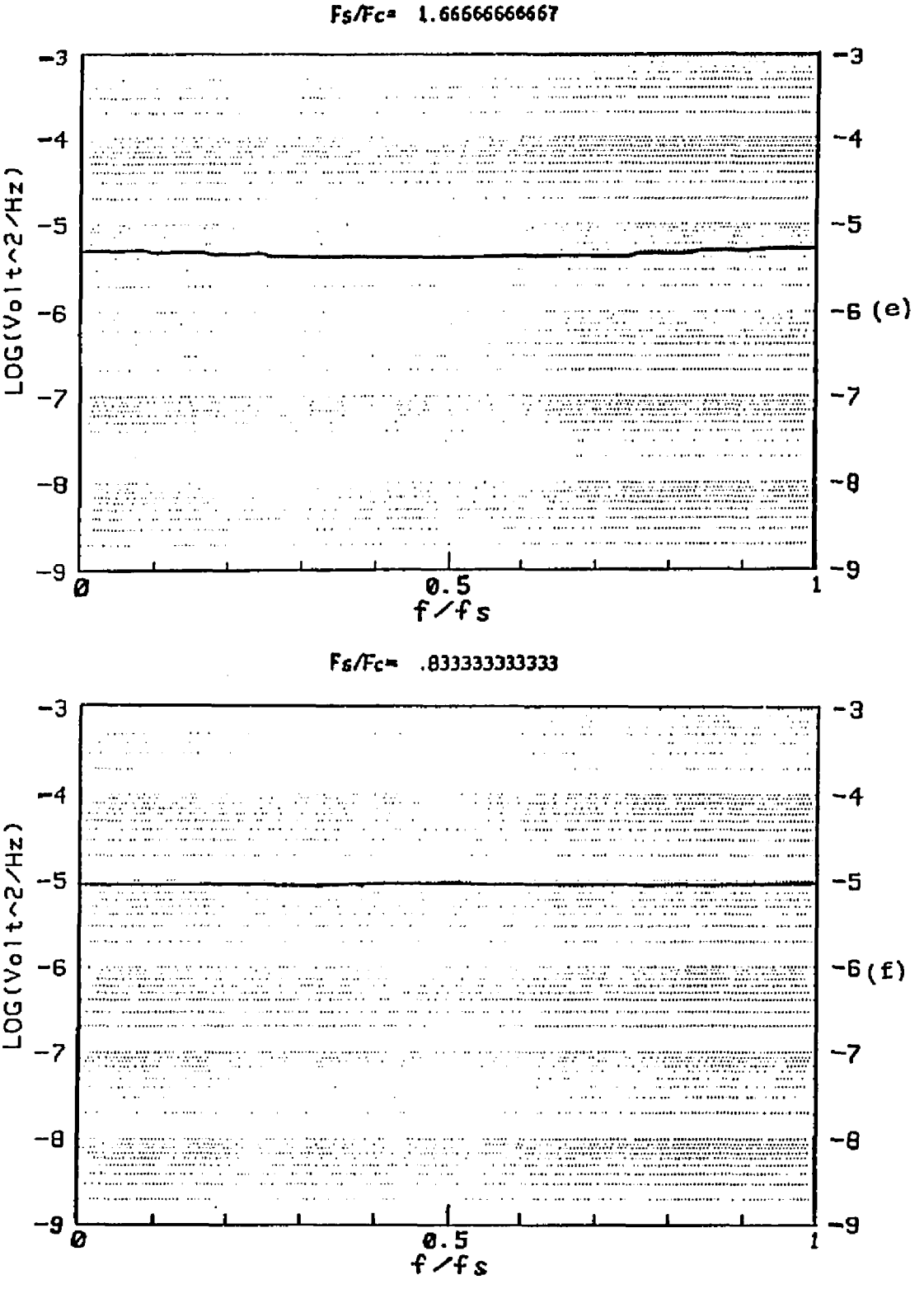

Fig. 4-4 Sampled Noise Spectrum with Different Ratios f_s/f_c

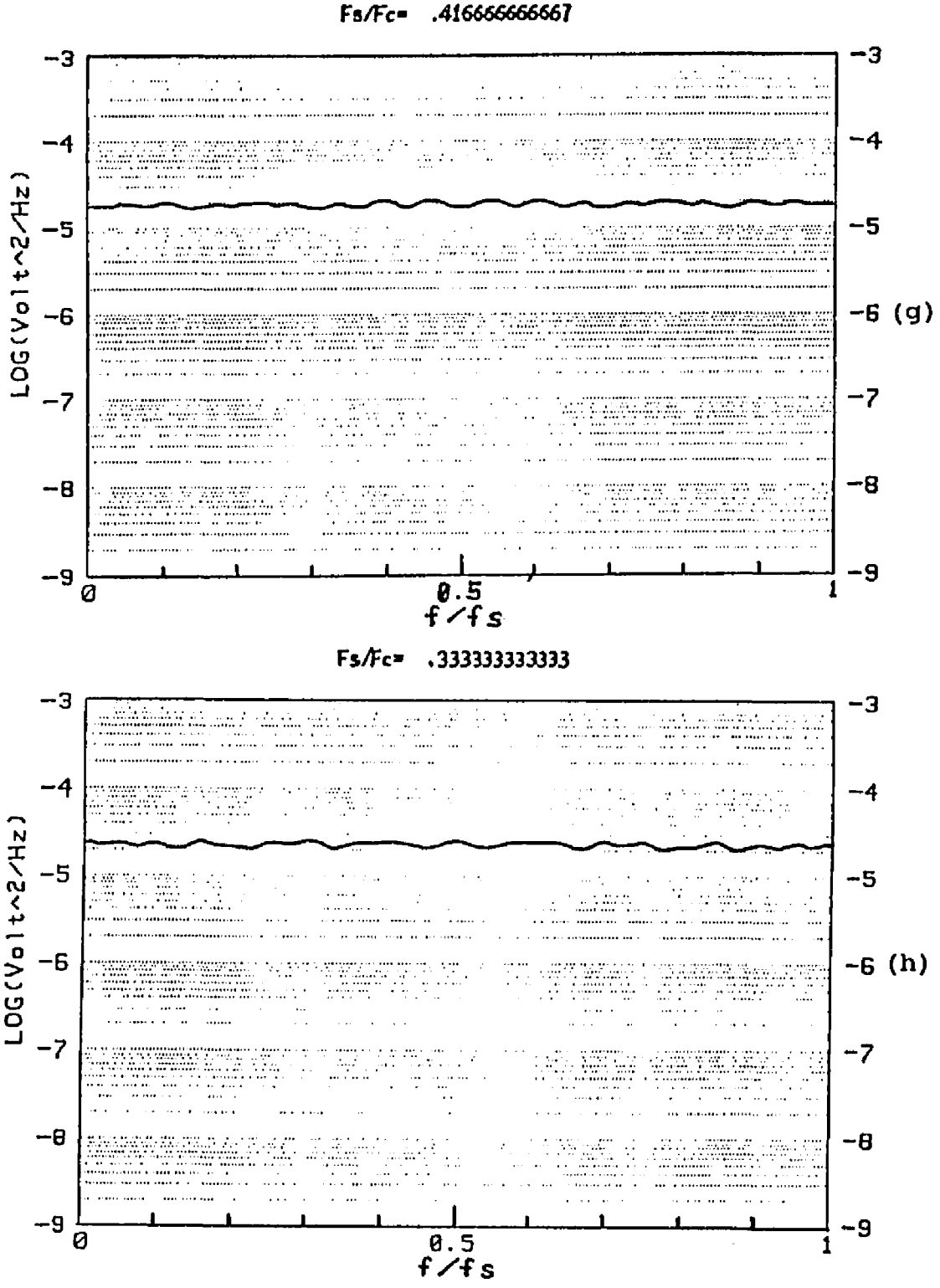

Fig. 4-4 Sampled Noise Spectrum with Different Ratios f_s/f_c

Next, the noise source is added to the reference level and a simple sampling and A/D conversion is made at the output of the simulated CCD output stage. The power spectrum of this output signal is illustrated in Fig. 4-5(b). From Fig. 4-5(b) one can see that it has very close characteristics with Fig. 4-5(a). It also shows that about 22% more power than that delivered by the noise source is present. This can be accounted to the noise contributed by the circuit components such as the MOS source follower.

Finally, the output signal is sampled by using the correlated double sampling technique instead of using simple sampling. The time interval between "clamp" and "sampling" is 2 μsec which is about one-half the sampling period (4 μsec). The power spectral density function after CDS is given in Fig. 4-5(c). It is observed that the power density is decreased by about 88% at low frequencies. Also, the total power is reduced by about 90%. Therefore, the effect of reducing noise by correlated double sampling is evident.

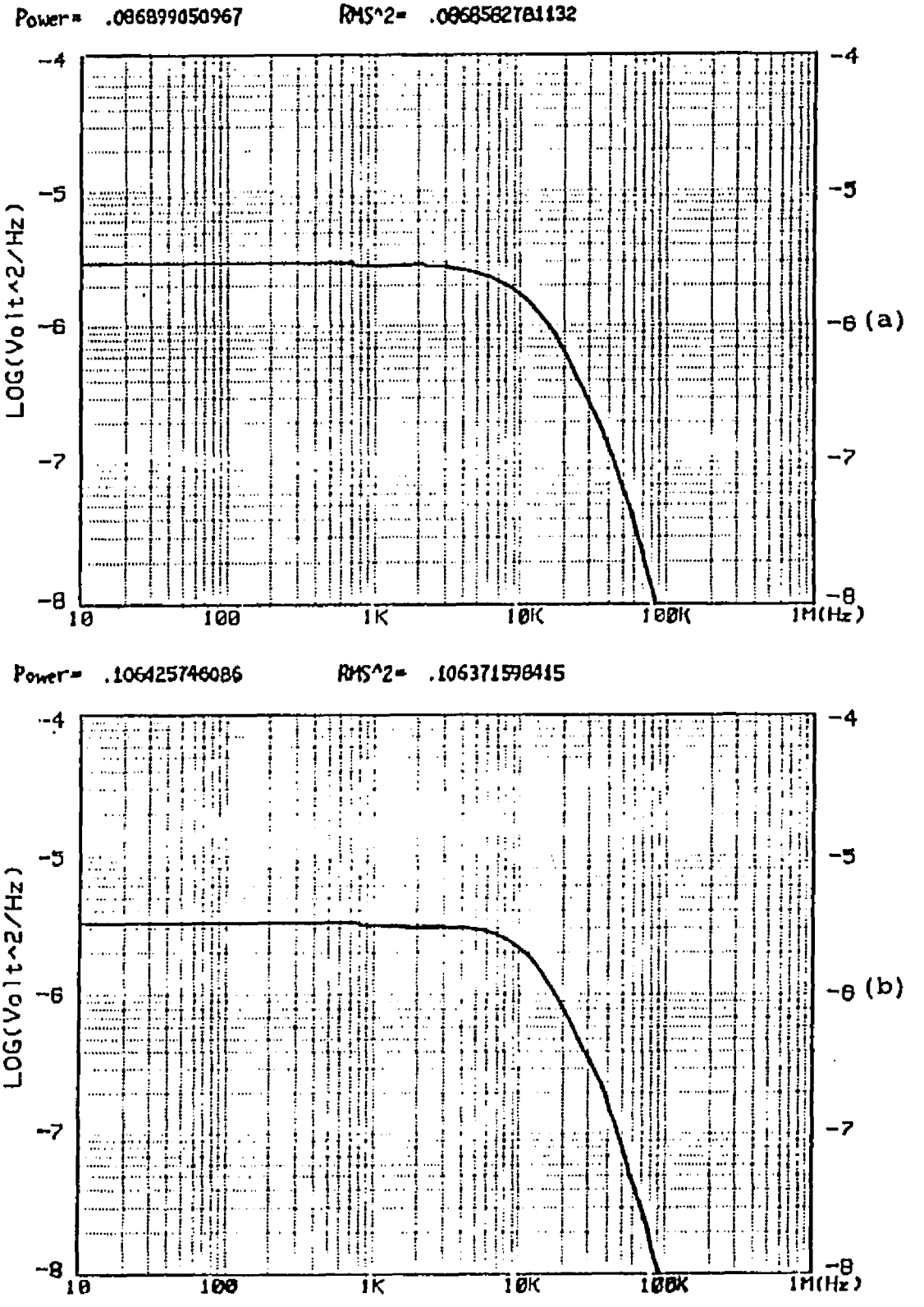

Fig. 4-5 (a) Noise Spectrum With Bandwidth of 15 kHz.
(b) Output Noise Spectrum Sampled by Simple Sampling.

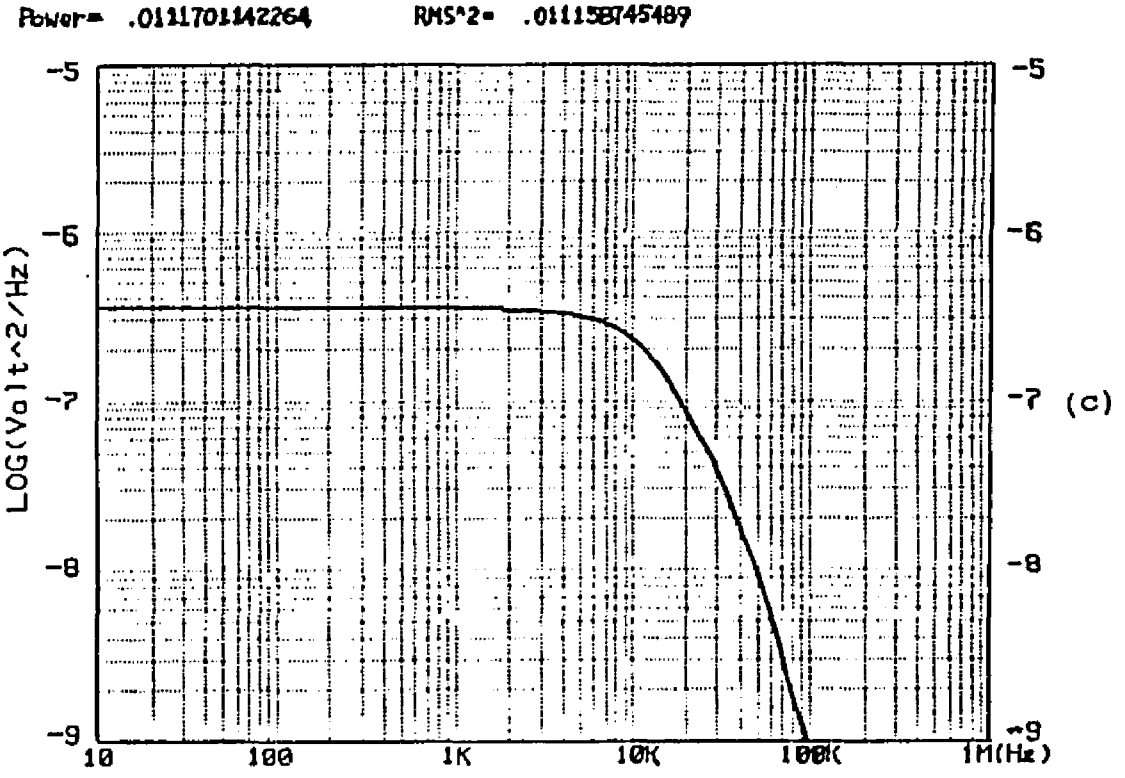

Fig. 4-5 (c) Output Noise Spectrum Sampled by CDS.

CHAPTER V CONCLUSION

5-1 Choosing Bandwidth of Low Pass Filter

It is evident from the previous chapters that by using the CDS technique, the reset noise from the reset switch can be removed, and the $1/f$ noise at low frequencies introduced by the on-chip MOS amplifier can be suppressed. Therefore, the dominant source of noise left in the readout circuitry is the thermal noise component generated in the on-chip MOS amplifier. If very low noise levels are required, careful optimization in the timing of the sampling pulses as well as introduction of appropriate filtering should be taken to eliminate the thermal noise contributed by the on-chip MOS amplifier. For understanding the tradeoff involved in this optimization, further analysis of the charge detection circuitry will be discussed in this section.

For convenience, Fig. 3-6 is redrawn as Fig. 5-1. It is stated in previous chapters that the CDS technique can reduce the reset noise contributed by reset switch M_1 and suppress the $1/f$ noise introduced by source follower M_2. Besides suppressing the $1/f$ noise of transistor M_2, the CDS circuit also affects the thermal noise component generated by this device. The purpose of the single pole low pass filter with

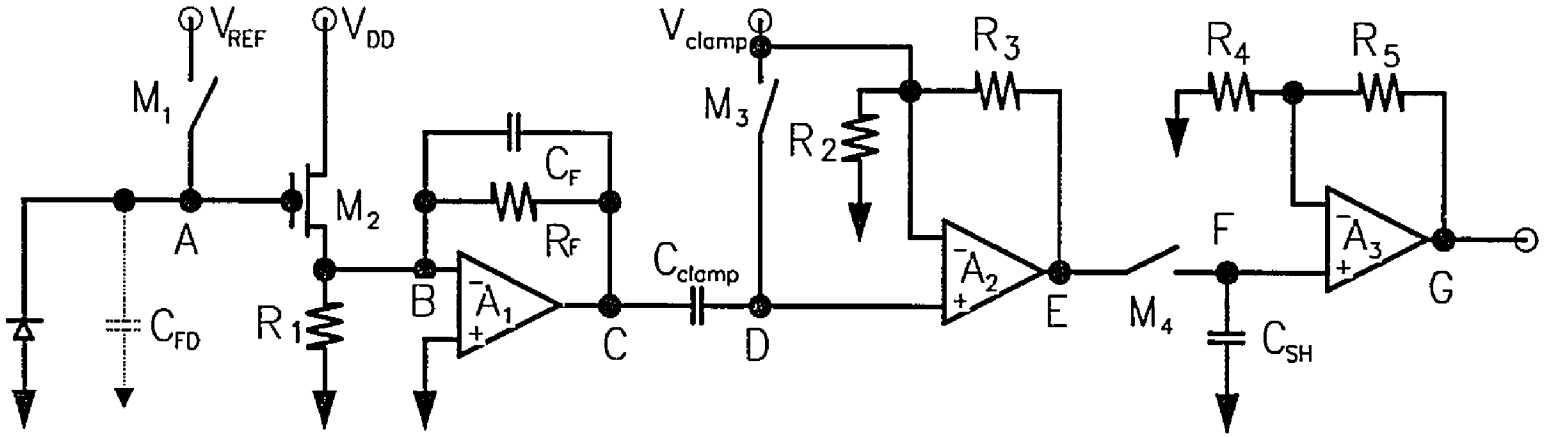

Fig. 5–1(a) Schematic diagram of a CDS processor.

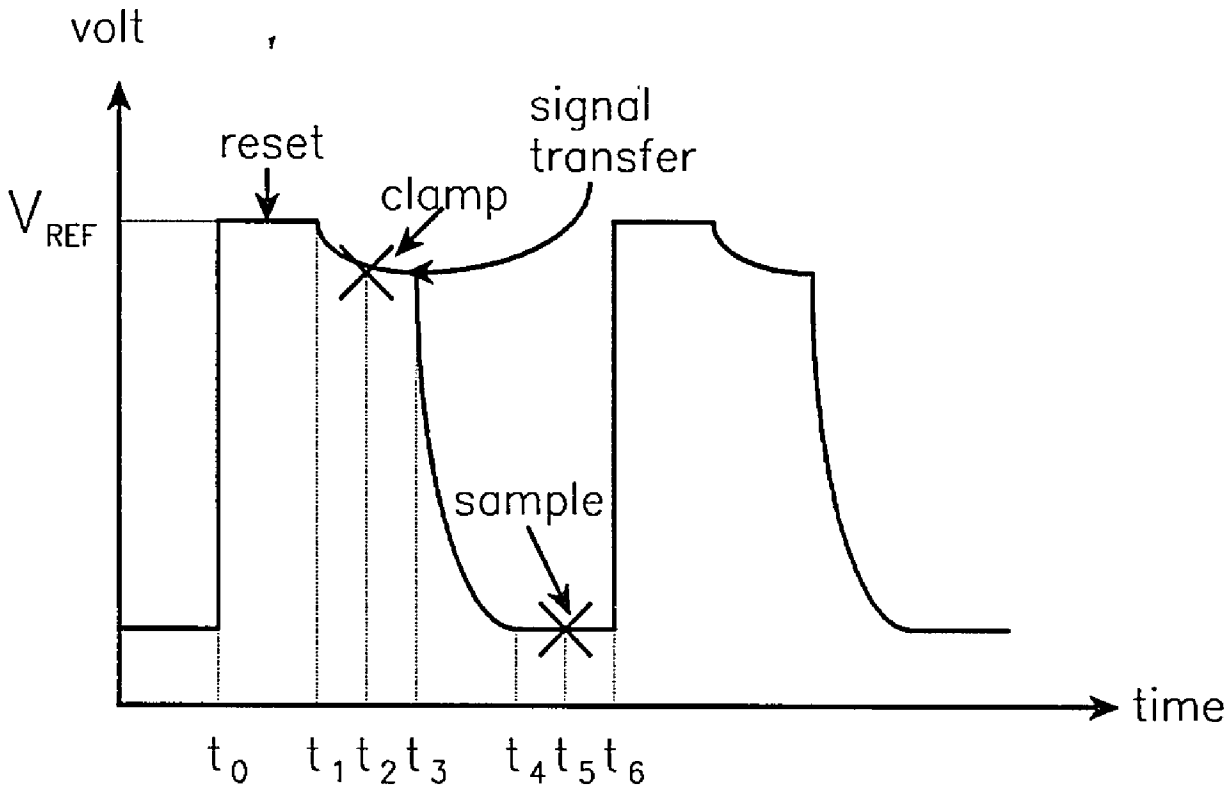

Fig. 5−1(b) Voltage waveform observed at point B in (a).

time constant $R_F C_F$ which follows M_2 in Fig. 5-1(a) is to bandlimit the thermal noise of transistor M_2 and thus, to introduce correlation of this noise between the two samples at t_2 and t_5. Taking this correlation into account, the resultant r.m.s. noise after bandlimiting and double sampling is given by[8]

$$\overline{V_n} = \overline{V_{H2}}\ (1/4R_FC_F)^{1/2}\cdot\{2[1-\exp(-\Delta\tau/R_FC_F)]\}^{1/2} \qquad (5\text{-}1)$$

where $\overline{V_{H2}}$ is the r.m.s. noise voltage from transistor M_2. From eq. (5-1) it can be seen that either decreasing the bandwidth of the R_FC_F filter (increasing the bandlimiting of the wide band noise V_{H2}) or decreasing the ratio $\Delta\tau/R_FC_F$, (increasing the correlation between the two samples), will result in a decreased noise level. Therefore, it would appear desirable to increase R_FC_F while decreasing the time between the clamp and sample pulse. However, as the time constant R_FC_F of the filter is increased, the voltage swing which represents the signal is attenuated by the factor, $1-\exp[-(t_4-t_3)/R_FC_F]$.

To maximize this factor, the largest possible amount of time should be given for the signal transient to occur. Therefore, the sample at t_5 should occur just before the following reset occurs at t_6 (see Fig 5-1(b)).

Another consideration which also limits the maximum size of R_FC_F is that a fraction $\exp[-(t_2-t_1)/R_{MOS}C_{FD}]$ of the reset noise introduced by switch M_1 will remain after the clamp has occurred because of the

correlation effects introduced by the bandlimiting. This fraction can be decreased by minimizing the width of the reset pulse ($t_1 \approx t_0$) and by clamping (i.e., the sample at t_2) just before the signal is transferred at t_3. Therefore, the tradeoff involved in choosing the bandwidth of the low pass filter, $R_F C_F$, is that the wide band noise of M2 should be bandlimited to as low a frequency as possible which implies a long time constant. However, this long time constant attenuates the signal swing as well as decreases the reset noise suppression.

A suitable compromise of the above considerations suggested by Brodersen and Emmons[8] is to allow three of four time constants ($R_F C_F$) between the reset and clamp pulses as well as between the signal transfer and the sample pulse. The optimum timing subject to this constraint is given by

$$t_1 - t_0 \ll T_s \tag{5-2}$$

$$t_2 - t_0 \approx t_3 - t_0 \tag{5-3}$$

$$t_5 - t_0 \approx T_s \tag{5-4}$$

where T_s is the sampling period. To obtain four time constants for the above mentioned intervals, the low pass filter should have a bandwidth, $f_{3dB} = 1/2\pi R_F C_F$, given by

$$f_{3dB} \approx 0.24\, f_s$$

where f_s is the sampling frequency.

5-2 SUMMARY

It has been shown that CDS provides a considerable noise reduction in the readout circuit of a CCD array. The main reason for using the CDS technique is to remove the reset noise contributed by the reset switch and to eliminate the $1/f$ noise introduced by the on-chip MOS amplifier. If very low noise levels are required, then the timing of the sampling pulses should be carefully optimized, and appropriate filtering should be implemented. There is a tradeoff between low noise levels and high signal swing ability involved in this optimization.

APPENDIX A DERIVATION OF EQUATION 2-12

$$V_{ds}(t) = V_{lp}(t) - V_{lp}(t-\Delta\tau).$$

$$\overline{V_{ds}^2} = \lim_{T\to\infty} \frac{1}{T}\int_{-T/2}^{T/2} V_{ds}^2(t)dt$$

$$= \lim_{T\to\infty} \frac{1}{T}\int_{-T/2}^{T/2} [V_{lp}(t)-V_{lp}(t-\Delta\tau)]^2 dt$$

$$= \lim_{T\to\infty} \frac{1}{T}\int_{-T/2}^{T/2} V_{lp}^2(t)dt$$

$$- \lim_{T\to\infty} \frac{2}{T}\int_{-T/2}^{T/2} V_{lp}(t)V_{lp}(t-\Delta\tau)dt$$

$$+ \lim_{T\to\infty} \frac{1}{T}\int_{-T/2}^{T/2} V_{lp}^2(t-\Delta\tau)dt.$$

If V_{lp} is stationary, then

$$\lim_{T\to\infty} \frac{1}{T}\int_{-T/2}^{T/2} V_{lp}^2(t-\Delta\tau)dt = \lim_{T\to\infty} \frac{1}{T}\int_{-T/2}^{T/2} V_{lp}^2(t)dt$$

and thus,

$$\overline{V_{ds}^2} = \lim_{T\to\infty} \frac{2}{T}\int_{-T/2}^{T/2} V_{lp}^2(t)dt - \lim_{T\to\infty} \frac{2}{T}\int_{-T/2}^{T/2} V_{lp}(t)V_{lp}(t-\Delta\tau)dt.$$

APPENDIX B TRANSFER FUNCTION OF THE DELAY-SUBTRACTOR MODEL

$$H(f) = \frac{Y(x)}{X(x)} .$$

If $x(t) = \delta(t)$, $y(t) = \delta(t)-\delta(t-\Delta\tau)$ and $X(x)$, $Y(x)$ are the Fourier transformations of $x(t)$ and $y(t)$, respectively, then

$$X(f) = \mathcal{F}\{x(t)\} = \mathcal{F}\{\delta(t)\} = 1$$

and

$$Y(f) = \mathcal{F}\{y(t)\} = \mathcal{F}\{\delta(t)-\delta(t-\Delta\tau)\} = 1 - e^{-j2\pi f\Delta\tau}.$$

Thus,

$$\begin{aligned} H(f) &= \frac{Y(x)}{X(x)} \\ &= 1 - e^{-j2\pi f\Delta\tau} \\ &= [1 - \cos(2\pi f\Delta\tau)] + j\sin(2\pi f\Delta\tau). \end{aligned}$$

Therefore,

$$\begin{aligned} |H(f)|^2 &= [1 - \cos(2\pi f\Delta\tau)]^2 + [\sin(2\pi f\Delta\tau)]^2 \\ &= 1 - 2\cos(2\pi f\Delta\tau) + \cos^2(2\pi f\Delta\tau) + \sin^2(2\pi f\Delta\tau) \end{aligned}$$

or

$$|H(f)|^2 = 2\cdot[1 - \cos(2\pi f\Delta\tau)] .$$

APPENDIX C DERIVATION OF EQUATION 2-17

$$V_{ds}(t) = V_{lp}(t) - V_{lp}(t-\Delta\tau).$$

$$\begin{aligned}
R_{ds}(\tau) &= \lim_{T\to\infty}\frac{1}{T}\int_{-T/2}^{T/2} V_{ds}(t)V_{ds}(t-\tau)dt \\
&= \lim_{T\to\infty}\frac{1}{T}\int_{-T/2}^{T/2} [V_{lp}(t)-V_{lp}(t-\Delta\tau)][V_{lp}(t-\tau)-V_{lp}(t-\tau-\Delta\tau)]dt \\
&= \lim_{T\to\infty}\frac{1}{T}\int_{-T/2}^{T/2} V_{lp}(t)V_{lp}(t-\tau)dt \\
&\qquad - \lim_{T\to\infty}\frac{1}{T}\int_{-T/2}^{T/2} V_{lp}(t)V_{lp}[t-(\tau+\Delta\tau)]dt \\
&\qquad\qquad - \lim_{T\to\infty}\frac{1}{T}\int_{-T/2}^{T/2} V_{lp}(t-\Delta\tau)V_{lp}[(t-\Delta\tau)-(\tau-\Delta\tau)]dt \\
&\qquad\qquad\qquad + \lim_{T\to\infty}\frac{1}{T}\int_{-T/2}^{T/2} V_{lp}(t-\Delta\tau)V_{lp}((t-\Delta\tau)-\tau)dt \\
&= R_{lp}(\tau)-R_{lp}(\tau+\Delta\tau)-R_{lp}(\tau-\Delta\tau)+R_{lp}(\tau)
\end{aligned}$$

or

$$R_{ds}(\tau) = 2R_{lp}(\tau)-R_{lp}(\tau+\Delta\tau)-R_{lp}(\tau-\Delta\tau).$$

APPENDIX D DERIVATION OF EQUATION 2-23

$$
\begin{aligned}
S_{icds} &= \frac{1}{T_s}\int_{-\infty}^{\infty}\delta_{Ts}(\tau)R_{ds}(\tau)\exp(-j2\pi f\tau)d\tau \\
&= \frac{1}{T_s}\sum_{n=-\infty}^{\infty}R_{ds}(nT_s)\exp(-j2\pi fnT_s) \\
&= \frac{2R_{1po}}{T_s}\sum_{n=-\infty}^{\infty}\exp(-|nT_s|/\tau_o)\exp(-j2\pi fnT_s) \\
&\quad - \frac{R_{1po}}{T_s}\sum_{n=-\infty}^{\infty}\exp(-|nT_s+\Delta\tau|/\tau_o)\cdot\exp(-j2\pi fnT_s) \\
&\quad - \frac{R_{1po}}{T_s}\sum_{n=-\infty}^{\infty}\exp(-|nT_s-\Delta\tau|/\tau_o)\cdot\exp(-j2\pi fnT_s). \qquad \text{(D-1)}
\end{aligned}
$$

The first term of eq. (D-1) is

$$
\begin{aligned}
&\frac{2R_{1po}}{T_s}\sum_{n=-\infty}^{\infty}\exp(-|nT_s|/\tau_o)\cdot\exp(-j2\pi fnT_s) \\
&= \frac{2R_{1po}}{T_s}\left[\ldots+\exp(-\frac{2T}{\tau_o})\exp(j2\pi f2T_s)+\exp(-\frac{T_s}{\tau_o})\exp(j2\pi fT_s)+1\right. \\
&\qquad\left. + \exp(-\frac{T_s}{\tau_o})\exp(-j2\pi fT_s)+\exp(-\frac{2T_s}{\tau_o})\exp(-j2\pi f2T_s)+\ldots\right] \\
&= \frac{2R_{1po}}{T_s}\left[\ldots+ 2\exp(-\frac{2T_s}{\tau_o})(\frac{e^{j2\pi f2T_s}+e^{-j2\pi f2T_s}}{2})\right. \\
&\qquad\left. + 2\exp(-\frac{T_s}{\tau_o})(\frac{e^{j2\pi fT_s}+e^{-j2\pi fT_s}}{2}) + 1\right] \\
&= \frac{2R_{1po}}{T_s}\left[\ldots+ 2\exp(-\frac{2T_s}{\tau_o})\cos(2\pi f2T_s)+2\exp(-\frac{T_s}{\tau_o})\cos(2\pi fT_s) + 1\right] \\
&= \frac{2R_{1po}}{T_s}\left[2\sum_{n=1}^{\infty}\exp(-\frac{nT_s}{\tau_o})\cos(2\pi fnT_s) + 1\right].
\end{aligned}
$$

Since $T_s \geq \Delta\tau$, we have that for $n < 0$

$$|nT_s - \Delta\tau| = -nT_s + \Delta\tau$$

$$|nT_s + \Delta\tau| = -(nT_s + \Delta\tau)$$

and for $n > 0$

$$|nT_s - \Delta\tau| = nT_s - \Delta\tau$$

$$|nT_s + \Delta\tau| = nT_s + \Delta\tau \ .$$

The expression of the second and third terms of eq. (D-1) can be written as following:

$$- \frac{R_{1po}}{T_s} \sum_{n=-\infty}^{\infty} \exp(-|nT_s+\Delta\tau|/\tau_o)\cdot\exp(-j2\pi f nT_s)$$

$$- \frac{R_{1po}}{T_s} \sum_{n=-\infty}^{\infty} \exp(-|nT_s-\Delta\tau|/\tau_o)\cdot\exp(-j2\pi f nT_s)$$

$$= - \frac{R_{1po}}{T_s} \left[\sum_{n=-\infty}^{\infty} \exp(-|nT_s+\Delta\tau|/\tau_o)\cdot\exp(-j2\pi f nT_s) + \sum_{n=-\infty}^{\infty} \exp(-|nT_s-\Delta\tau|/\tau_o)\cdot\exp(-j2\pi f nT_s) \right] \qquad \text{(D-2)}$$

in which

$$\sum_{n=-\infty}^{\infty} \exp(-|nT_s+\Delta\tau|/\tau_o)\cdot\exp(-j2\pi f nT_s) + \sum_{n=-\infty}^{\infty} \exp(-|nT_s-\Delta\tau|/\tau_o)\cdot\exp(-j2\pi f nT_s)$$

$$= \ldots + \exp(-\frac{+2T_s-\Delta\tau}{\tau_o})\exp(j2\pi f 2T_s) + \exp(-\frac{+T_s-\Delta\tau}{\tau_o})\exp(j2\pi f T_s) + \exp(-\frac{\Delta\tau}{\tau_o})$$

$$+ \exp(-\frac{T_s+\Delta\tau}{\tau_o})\exp(-j2\pi f T_s) + \exp(-\frac{2T_s+\Delta\tau}{\tau_o})\exp(-j2\pi f 2T_s) + \ldots$$

$$+ \ldots + \exp(-\frac{2T_s+\Delta\tau}{\tau_o})\exp(j2\pi f 2T_s) + \exp(-\frac{T_s+\Delta\tau}{\tau_o})\exp(j2\pi f T_s) + \exp(-\frac{\Delta\tau}{\tau_o})$$

$$+ \exp(-\frac{T_s-\Delta\tau}{\tau_o})\exp(-j2\pi f T_s) + \exp(-\frac{2T_s-\Delta\tau}{\tau_o})\exp(-j2\pi f 2T_s) + \ldots \qquad \text{(D-3)}$$

After rearrangement, eq. (D-3) can be written as

$$\ldots+2\exp\left(-\frac{2T_s-\Delta\tau}{\tau_o}\right)\left[\frac{\exp(+j2\pi f2T_s)+\exp(-j2\pi f2T_s)}{2}\right]$$

$$+2\exp\left(-\frac{T_s-\Delta\tau}{\tau_o}\right)\left[\frac{\exp(+j2\pi fT_s)+\exp(-j2\pi fT_s)}{2}\right]$$

$$+2\exp\left(-\frac{T_s+\Delta\tau}{\tau_o}\right)\left[\frac{\exp(-j2\pi fT_s)+\exp(+j2\pi fT_s)}{2}\right]$$

$$+2\exp\left(-\frac{2T_s+\Delta\tau}{\tau_o}\right)\left[\frac{\exp(-j2\pi f2T_s)+\exp(+j2\pi f2T_s)}{2}\right]+2\exp\left(-\frac{\Delta\tau}{\tau_o}\right)$$

$$= 2\sum_{n=1}^{\infty}\exp\left(-\frac{nT_s-\Delta\tau}{\tau_o}\right)\cos(2\pi fnT_s)+2\sum_{n=1}^{\infty}\exp\left(-\frac{nT_s+\Delta\tau}{\tau_o}\right)\cos(2\pi fnT_s)+2\exp\left(-\frac{\Delta\tau}{\tau_o}\right)$$

$$= 2\exp\left(\frac{\Delta\tau}{\tau_o}\right)\sum_{n=1}^{\infty}\exp\left(-\frac{nT_s}{\tau_o}\right)\cos(2\pi fnT_s)+2\exp\left(-\frac{\Delta\tau}{\tau_o}\right)\sum_{n=1}^{\infty}\exp\left(-\frac{nT_s}{\tau_o}\right)\cos(2\pi fnT_s)$$

$$+ 2\exp\left(-\frac{\Delta\tau}{\tau_o}\right)$$

$$= \exp\left(-\frac{\Delta\tau}{\tau_o}\right)\left[1+2\sum_{n=1}^{\infty}\exp\left(-\frac{nT_s}{\tau_o}\right)\cos(2\pi fnT_s)\right]+\exp\left(-\frac{\Delta\tau}{\tau_o}\right)$$

$$+\exp\left(\frac{\Delta\tau}{\tau_o}\right)\left[1+2\sum_{n=1}^{\infty}\exp\left(-\frac{nT_s}{\tau_o}\right)\cos(2\pi fnT_s)\right]-\exp\left(\frac{\Delta\tau}{\tau_o}\right)$$

$$= \left[1+2\sum_{n=1}^{\infty}\exp\left(-\frac{nT_s}{\tau_o}\right)\cos(2\pi fnT_s)\right]\left[\exp\left(-\frac{\Delta\tau}{\tau_o}\right)+\exp\left(\frac{\Delta\tau}{\tau_o}\right)\right]+\left[\exp\left(-\frac{\Delta\tau}{\tau_o}\right)-\exp\left(\frac{\Delta\tau}{\tau_o}\right)\right].$$

Therefore (D-2) can be rewritten as

$$-\frac{R_1 p_o}{T_s}\left\{\left[1+2\sum_{n=1}^{\infty}\exp\left(-\frac{nT_s}{\tau_o}\right)\cos(2\pi fnT_s)\right]\left[\exp\left(-\frac{\Delta\tau}{\tau_o}\right)+\exp\left(\frac{\Delta\tau}{\tau_o}\right)\right]\right.$$

$$\left.+\left[\exp\left(-\frac{\Delta\tau}{\tau_o}\right)-\exp\left(\frac{\Delta\tau}{\tau_o}\right)\right]\right\}.$$

Thus,

$$S_{icds} = \frac{R_{ipo}}{T_s}\left\{\left[1+2\sum_{n=1}^{\infty}\exp(-\frac{nT_s}{\tau_o})\cos(2\pi fnT_s)\right]\left(2-[\exp(-\frac{\Delta\tau}{\tau_o})+\exp(\frac{\Delta\tau}{\tau_o})]\right)\right.$$
$$\left.-\left[\exp(-\frac{\Delta\tau}{\tau_o})-\exp(\frac{\Delta\tau}{\tau_o})\right]\right\}$$

in which

$$1 + 2\sum_{n=1}^{\infty}\exp(-\frac{nT_s}{\tau_o})\cos(2\pi fnT_s) = \frac{\sinh(T_s/\tau_o)}{\cosh(T_s/\tau_o)-\cos(2\pi fT_s)} \quad [9]$$

and

$$2 - [\exp(-\frac{\Delta\tau}{\tau_o})+\exp(\frac{\Delta\tau}{\tau_o})] = 2 - 2\left[\frac{\exp(-\frac{\Delta\tau}{\tau_o})+\exp(\frac{\Delta\tau}{\tau_o})}{2}\right]$$

$$= 2[1-\cosh(\Delta\tau/\tau_o)]$$

and

$$\exp(-\frac{\Delta\tau}{\tau_o}) - \exp(\frac{\Delta\tau}{\tau_o}) = -2\sinh(\frac{\Delta\tau}{\tau_o}).$$

Therefore,

$$S_{icds} = \frac{2R_{ipo}}{T_s}\left[\frac{\sinh(T_s/\tau_o)}{\cosh(T_s/\tau_o) - \cos(2\pi fT_s)}\cdot[1 - \cosh(\Delta\tau/\tau_o)]+\sinh(\Delta\tau/\tau_o)\right].$$

REFERENCES

[1] J. E. Carnes and W. F. Kosonocky, "Noise Sources in Charge-Coupled Devices," *RCA Rev.*, Vol. 33, pp. 327, 1972.

[2] A. Van Der Ziel, "Noise in Solid-state Devices and Lasers," *Proc. IEEE*, Vol. 58, pp. 1178 - 1206, 1970.

[3] F. R. Conner, *Noise*, Edward Arnold, 1973.

[4] C. A. Gobert, "Spectral Distribution of a Sampled First-Order Lowpass Filtered White Noise," *Electronics Letters*, Vol.17, No.19, pp.720-721, 1981.

[5] D. F. Barbe, "Imaging Devices Using the Charge-Coupled Concept," *Proc. of IEEE*, Vol. 63, No. 1, pp. 38-66, 1975.

[6] M. H. White, United States Patent 3,781,574,1973.

[7] S. M. Kay and S. L. Marple, Jr., "Spectrum Analysis—a Modern Perspective," *Proc. IEEE*, Vol. 69, No. 11, pp. 1380-1419, Nov. 1981.

[8] R. W. Brodersen and S. P. Emmons, "The Measurement of Noise in Buried Channel Charge Coupled Devices," *Proc. Int. Conf. Appl. of CCD's*, (San Diego, CA), 1975.

[9] I. S. Gradshteyn and I. M. Ryzhik, *Table of Integrals, Series, and Products*, Academic Press, 1979, pp. 42.

[10] L. Marple, "A New Autoregressive Spectrum Analysis Algorithm," *IEEE Trans. Acoust., Speech, Signal Process.*, Vol. ASSP-28, No. 4, pp. 441-454, Aug. 1980.